Title

Sum-Rule Constraints on the Surface State Conductance of Topological Insulators

Journal

Physical Review Letters, 115(11)

ISSN

0031-9007

Authors

Post, KW
Chapler, BC
Liu, MK
et al.

Publication Date

2015-09-11

DOI

10.1103/physrevlett.115.116804

Peer reviewed

Sum-Rule Constraints on the Surface State Conductance of Topological Insulators

K. W. Post,[1,*] B. C. Chapler,[1] M. K. Liu,[1] J. S. Wu,[1] H. T. Stinson,[1] M. D. Goldflam,[1] A. R. Richardella,[2] J. S. Lee,[2] A. A. Reijnders,[3] K. S. Burch,[4] M. M. Fogler,[1] N. Samarth,[2] and D. N. Basov[1]

[1]*Physics Department, University of California-San Diego, La Jolla, California 92093, USA*

[2]*Department of Physics, The Pennsylvania State University, University Park, Pennsylvania 16802, USA*

[3]*Department of Physics & Institute for Optical Sciences, University of Toronto, Toronto, Ontario M5S 1A7, Canada*

[4]*Department of Physics, Boston College, Chestnut Hill, Massachusetts 02467, USA*

(Received 3 June 2014; revised manuscript received 5 July 2015; published 11 September 2015)

We report the Drude oscillator strength D and the magnitude of the bulk band gap E_g of the epitaxially grown, topological insulator $(Bi,Sb)_2Te_3$. The magnitude of E_g, in conjunction with the model independent f-sum rule, allows us to establish an upper bound for the magnitude of D expected in a typical Dirac-like system composed of linear bands. The experimentally observed D is found to be at or below this theoretical upper bound, demonstrating the effectiveness of alloying in eliminating bulk charge carriers. Moreover, direct comparison of the measured D to magnetoresistance measurements of the same sample supports assignment of the observed low-energy conduction to topological surface states.

DOI: 10.1103/PhysRevLett.115.116804 PACS numbers: 73.50.-h, 73.25.+i, 78.30.-j

The prediction and discovery of Dirac-like gapless surface states (SSs) (see Fig. 1) at the interface between a topological insulator (TI) and a trivial insulator have vaulted TIs to the vanguard of condensed matter physics [1]. Surface probes such as angle resolved photoemission spectroscopy and scanning tunneling spectroscopy have been extremely successful in verifying and discovering novel phenomena associated with the SSs (e.g., Refs. [2–5]). However, progress in the field has been plagued by native defects, resulting in significant concentrations of bulk charge carriers. These bulk dopants inhibit isolation and utilization of SS phenomena [6]. In order to realize many of the novel scientific and technological advances that could blossom from the unique electronic, spin, and optical properties of SSs in TIs, it is paramount to eliminate the bulk dopants.

Two archetypal strong TIs (topological invariant $\nu_0 = 1$ [1]) that are known to suffer from materials issues related to bulk dopants are Bi_2Te_3 and Sb_2Te_3. However, epitaxial films of Bi_2Te_3 can be n-type bulk conductors [6,7], whereas Sb_2Te_3 films are p-type bulk conductors [8]. Based on this observation, TI materials have been grown where the ratio Bi:Sb in $(Bi,Sb)_2Te_3$ (BST) is tuned to produce a compensated material with bulk insulating properties [9–11]. Here, we prove, using optical spectroscopy, the acute effectiveness of alloying in reducing or eliminating bulk charge carriers. The advantage of our optical experiments is that they give direct access to the frequency dependent electrodynamic response of free carriers in a metal via the Drude peak. In our $(Bi,Sb)_2Te_3$ film we find the Drude oscillator strength D sufficiently low as to lie at or below the upper bound that is theoretically anticipated for an isolated Dirac SS Drude response (i.e., a Drude response with no bulk contribution) (see Table I). These infrared data are complemented by the charge carrier density n and mobility μ from Hall effect measurements, as well as the magnetoresistance, which are all consistent with low-energy conduction arising from the topological SS.

We begin by describing the optical response of Dirac electrons in a strong TI, neglecting potential interband bulk $\rightarrow$ SS transitions (or vice versa) [15]. The simplest Dirac electron system is composed of linear bands (LB), without spin or valley degeneracy, where the dispersion is given by $E(k) = kv_F$, as illustrated schematically in Figs. 1(a) and 1(b). In this system, the total conductance $G^{\mathrm{LB}}_{\mathrm{tot}}$ is the sum of an intraband $G^{\mathrm{LB}}_{\mathrm{intra}}(\omega)$ and an interband $G^{\mathrm{LB}}_{\mathrm{inter}}(\omega)$ component. When the Fermi energy E_F is at the Dirac point, theory predicts that SS interband transitions give rise to a frequency independent conductance of $G^{\mathrm{LB}}_{\mathrm{inter}} = \frac{1}{8}(\pi e^2/h)$ [16]. However, the area of the Fermi surface is zero, yielding $G^{\mathrm{LB}}_{\mathrm{intra}} = 0$. When E_F is shifted away from the Dirac point, empty states suppress interband transitions at energies below $2|E_F|$, as illustrated in Fig. 1(b), resulting in $G^{\mathrm{LB}}_{\mathrm{inter}}(\omega) = 0$ for $\omega < 2|E_F|$. Importantly, the f-sum rule [17] demands that the total spectral weight of the Dirac electrons $\int_0^\infty G^{\mathrm{LB}}_{\mathrm{tot}} d\omega$ be conserved [18,19]. Therefore, the loss of spectral weight in $G^{\mathrm{LB}}_{\mathrm{inter}}(\omega)$ must be compensated by a gain in $G^{\mathrm{LB}}_{\mathrm{intra}}(\omega)$, leading to

$$G^{\mathrm{LB}}_{\mathrm{inter}} 2|E_F| = \int_0^\infty G^{\mathrm{LB}}_{\mathrm{intra}} \hbar d\omega. \tag{1}$$

It is customary to express the relationship between intraband spectral weight and Drude oscillator strength D^s_{LB} as

$$\int_0^\infty G_{\mathrm{intra,LB}}(\omega)\hbar d\omega = \frac{\pi}{30\Omega} D^s_{\mathrm{LB}}, \tag{2}$$

which implies the simple relationship between E_F and D^s_{LB}

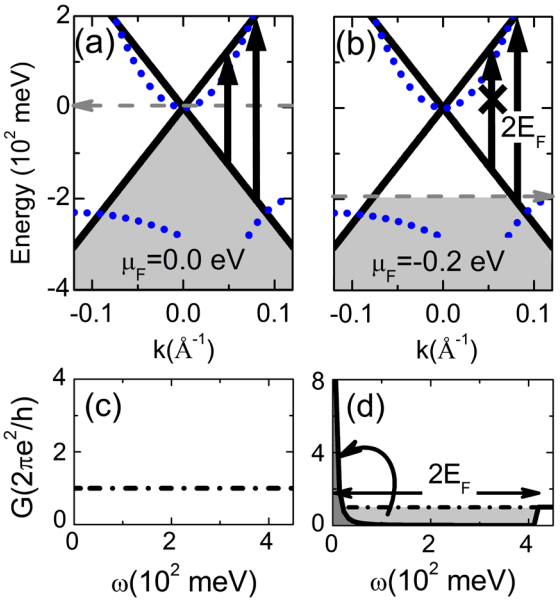

FIG. 1 (color online). Panels (a) and (b) show the band structure of a model TI, where the SS is composed of simple linear bands. The bulk band structure is also indicated by the dotted blue lines, consisting of two hole bands and an electron band. In (a) E_F is at the Dirac point, while in (b) E_F is 0.20 eV below the Dirac point, where the arrows in both panels schematically show the allowed transitions. In (a), interband transitions are allowed at all energies, giving rise to the conductance spectra shown in (c). When E_F is shifted below the Dirac point, transitions cannot occur from the depopulated region. Thus, transitions are suppressed below $2|E_F|$, giving rise to the conductance spectra shown in (d).

$$D^s_{\mathrm{LB}} = \frac{60\Omega}{\pi} G^{\mathrm{LB}}_{\mathrm{inter}} |E_F|. \tag{3}$$

The conductivity of the TI is dominated by the surface states, provided E_F is located outside of the bulk bands. It is customary to measure E_F relative to the Dirac point. Then, for p-type conductivity, E_F, defined relative to the Dirac point, cannot lie within the bulk bands. Therefore, for p-type (n-type) SS conduction, the maximum value of D^s_{LB}, occurs when the Dirac point is at the conduction band minimum (valence band maximum), and E_F is at the valence band maximum (conduction band minimum). Then, the energy that corresponds to the maximum value of E_F is simply E_g, with the maximum value of D^s_{LB}, $D^s_{\mathrm{LB,max}}$, given by $D^s_{\mathrm{LB,max}} = (N_S)(60\Omega/\pi)G_{\mathrm{TI}}E_g$, where N_S is the number of probed interfaces between systems with different topological indices. Here, $N_S = 2$ since optical transmission probes two topological surfaces, i.e., the interface between the film and the vacuum, and that between the film and the substrate.

The straightforward relationship between D_{LB} and E_F in Eq. (3) is useful for estimating the Drude spectral weight that could arise from SSs, and for intuitively understanding the spectral weight transfer in TI systems. Importantly, the resilience of the f-sum rule to external parameters has been experimentally verified numerous times in a prototypical surface state conductor: graphene. Even with gating, where additional charge carriers are introduced, the f-sum rule is found to be correct within the experimental error bars [20]. The reason for this is that the dominant effect of gating is a redistribution of spectral weight, while the increase in carriers is a relatively small perturbation. Importantly, TI materials are often not well modeled by linear bands. Instead, significant hexagonal warping effects are observed in Bi_2Te_3 and $(Bi,Sb)_2Te_3$ as well as asymmetry between the upper and lower portions of the Dirac cone [4,9]. These combined effects modify the conductance from the constant value shown in Fig. 1(c), and therefore change the value of D^s for a given E_F [16]. To more accurately estimate D^s_{max}, we have considered the optical response of a more realistic SS dispersion of a similarly doped sample [9,16]. This additional analysis suggests that D^s_{max} could be enhanced by approximately 25%, depending on the sample in question [21].

TABLE I. Bulk band gap E_g, experimental Drude oscillator strength D from transmission based experiments, modeled Drude oscillator strength D^s_{3layer} where the conductance is assumed to be from two topological surfaces with an insulating bulk, and theoretical upper bound of the free Dirac SS Drude oscillator strength $D^s_{\mathrm{LB,max}}$ of prototypical strong TIs obtained using the bulk energy gap, and assuming bands with linear dispersion. Values of D are all taken from low-temperature data (6–20 K). All units are in meV.

TI material	E_g	D	D^s_{3layer}	$D^s_{\mathrm{LB,max}}$	References
Bi_2Se_3	300	0.5–0.70	⋯	0.17	[2,12]
Bi_2Te_3	142	1.26	⋯	0.08	[7]
$Bi_{1.5}Sb_{0.5}Te_{1.8}Se_{1.2}$	340	1.42	⋯	0.20	[13]
Bi_2Te_2Se[a]	290	⋯	0.83	0.08	[10]
$Bi_{0.92}Sb_{1.08}Te_3$	207	0.13	0.14	0.12	This work
Bi_2Se_3	300	0.09	⋯	0.17	[14]

[a]The results of Ref. [10] are from reflection based experiments, and thus only one topological surface is considered.

In light of the constraints on D imposed by the f-sum rules, we experimentally determined D and E_g of $(Bi,Sb)_2Te_3$ through a combination of terahertz time-domain spectroscopy and Fourier transform infrared spectroscopy (FTIR). Details of the sample growth and experimental techniques are included in Ref. [21]. In Fig. 2(a), we plot the frequency dependent conductance spectra $G(\omega)$ [real part of $\tilde{\sigma}(\omega) \times$ thickness] of our $(Bi,Sb)_2Te_3$ film from 2–18 meV, the relevant energy scale for the Drude response. The most prominent feature at all temperatures is the narrow resonance centered near 6 meV, which is attributed to a phonon. There is another, weaker phonon resonance, slightly higher in energy, at roughly 8 meV. The assignment of these phonon modes is discussed in Ref. [21] At energies below these features, we observe a relatively flat but finite $G(\omega)$ related to the Drude response.

To quantify the Drude oscillator strength D, we construct a Drude-Lorentz model to describe the conductance of the BST system:

$$G(\omega) = \frac{1}{15\Omega}\frac{D\tau}{1+(\omega\tau)^2} + \sum_{j=1}^{n}\frac{A_j\Gamma_j\omega^2}{(\omega^2-\omega_{0j}^2)^2+(\Gamma_j\omega)^2}, \tag{4}$$

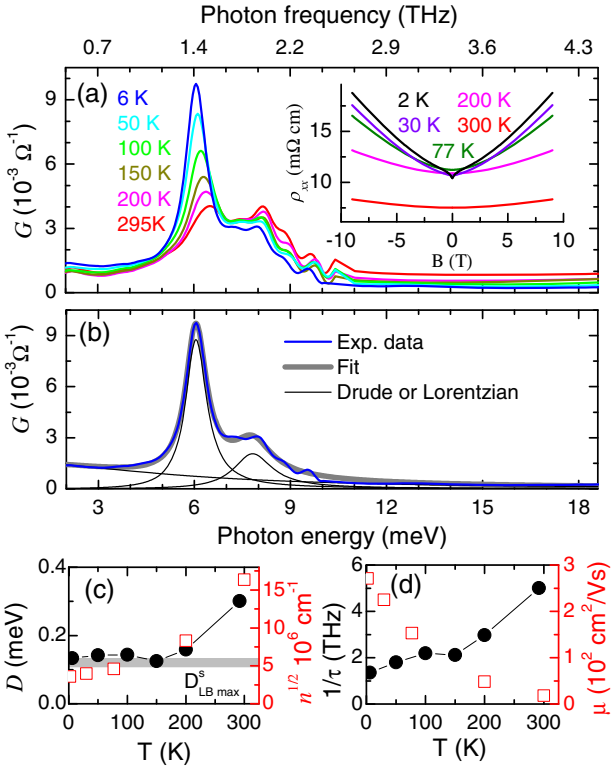

FIG. 2 (color online). (a) Temperature dependent spectrum of the conductance of $(Bi, Sb)_2Te_3$ obtained from terahertz time-domain spectroscopy and FTIR. The inset shows (symmetrized) dc magnetoresistivity data for this film. The "cusp" at the low-B field in the 2 K data is indicative of weak antilocalization. (b) Drude-Lorentz model fit (4) (gray) of the 6 K experimental conductance (blue). Individual Drude or Lorentzian oscillators are displayed as thin black lines. (c) Temperature dependence of the Drude oscillator strength D (black points) corresponding to the left axis, and square root of the charge carrier density n (open red squares) extracted from Hall effect measurements, corresponding to the right axis. The upper bounds for the Drude response of the linear SS ($D^s_{\mathrm{LB,max}} \pm 10\%$), and more realistic estimate of the SS contribution including hexagonal warping ($D^s_{\mathrm{BST,max}}$) in $(Bi, Sb)_2Te_3$, are indicated by the light gray and dark gray bars, respectively. (d) Temperature dependence of the free carrier scattering rate $1/\tau$ from optics (black points, left axis) and charge mobility μ from Hall effect measurements (open red squares, right axis).

where the first term describes the Drude response and the second term corresponds to Lorentzian resonances with amplitude A, width Γ, and center frequency ω_0. A representative Drude-Lorentz model fit is shown in Fig. 2(b) for the 6 K spectrum. The Drude-Lorentz models and the corresponding data at higher temperatures are shown in Ref. [21]. To independently confirm the values of D obtained from the model, we also considered a multilayer model where the BST system consisted of two conducting surface layers and an insulating bulk [21]. The Drude oscillator strength attributed to these conducting surface layers was consistent with the value of D extracted from the measured $G(\omega)$ spectra.

Above 150 K, both D and $1/\tau$ for $(Bi, Sb)_2Te_3$ [black points in Figs. 2(c) and 2(d)] decrease as temperature is reduced. Since $D \propto \sqrt{n}$, for 2D Dirac states, the reduction in D indicates a reduction in charge carriers, consistent with thermal activation at higher temperatures.The charge carrier density n extracted from Hall effect measurements on this film indicates p-type conduction, as is typical of $(Bi_{1-x}Sb_x)_2Te_3$ systems [9,11], with thermal activation at $T > 150$ K [open red squares in Fig. 2(c)]. Moreover, the magnetoresistance data at 200 and 300 K, shown in the inset to Fig. 2(a), show a nonlinear trend with magnetic field B, suggesting multiband transport, also consistent with the notion of thermally activated bulk states coexisting with SSs. Furthermore, since thermally activated charge carriers are not topologically protected, it is likely that their presence would yield a lower mobility (larger $1/\tau$). Therefore, the simultaneous decrease in D and $1/\tau$ as the temperature is lowered, supports the notion that thermally activated charge carriers are frozen out, leaving only high mobility carriers. The Hall parameters n and μ for these high temperature data in Fig. 2 were fit only in the linear regime (-1 T $< B <$ 1 T).

Below 150 K, D and $1/\tau$ remain relatively constant near 0.13 meV and 2 THz, respectively. Importantly, our low temperature D value lies right at the threshold of $D^s_{\mathrm{LB,max}} \pm 10\%$ for $(Bi, Sb)_2Te_3$, indicated by the light gray bar in Fig. 2(c). This latter fact indicates that the measured Drude spectral weight is consistent with a SS dominated response. Moreover, the low temperature value of D is roughly 5 to 10 times lower than most of those previously reported for other representative TIs (see Table I), with the exception of a recent report for Cu-doped Bi_2Se_3 [14]. The next lowest experimentally measured D come from Bi_2Se_3 [12], in which the D values suggest E_F is in the bulk conduction band. However, in this latter case, corrections to the Bi_2Se_3 SS band structure mentioned earlier [12] and the persistence of 2D topological SSs to well above the conduction band minimum [35] do imply that D is consistent with a significant SS transport component in Bi_2Se_3.

To verify that the measured parameters $D^{\mathrm{exp}} = 0.13$ meV and $n^{\mathrm{exp}}_{\mathrm{2D}} = 1.3 \times 10^{13}$ cm^{-2} are consistent with surface dominated transport, we can compare our results to that expected from experimentally obtained SS dispersion of TI materials with a similar $(Bi, Sb)_2Te_3$ composition [9,11]. For this comparison we will utilize Eq. (3) and the relationship between E_F and the carrier density of a single surface (n_{SS}) [20]

$$E_F = \hbar v_0 \sqrt{4\pi n_{\mathrm{SS}}} \tag{5}$$

to directly relate E_F, n_{SS}, and D via

$$D^s_{\mathrm{LB}} = (N_s)\frac{60\Omega}{\pi} G_{\mathrm{TI}} \hbar v_0 \sqrt{4\pi n_{\mathrm{SS}}}. \tag{6}$$

For direct comparison between transport and optics, we use $n_{\mathrm{SS}} = n^{\mathrm{exp}}_{\mathrm{2D}}/2$, assuming the carriers were divided between two surfaces and $v_0 = 3.8 \times 10^5$ m/s, consistent with both

photoemission and transport measurements of p-type SS carriers [11,36]. These values yield $D^s_{\mathrm{LB}} = 0.13$ meV, exactly reproducing our measured value. Moreover, this analysis corresponds to $E_F = 0.22$ eV, in close agreement with the measured E_G of 0.206 eV, suggesting the optical response is close to the constraints imposed by the sum rule analysis. If the additional contribution to D from the bulk bands is taken into account, in the regime where $E_F \approx E_G$, we recover our experimentally measured value of D when $E_F = 0.211$ eV. This analysis, which is detailed in Ref. [21], suggests E_F penetrates only up to 5 meV into the bulk bands, and bulk carriers constitute only 2% of the total $n_{2\mathrm{D}}$. Hexagonal warping, and other modifications to the SS dispersion, discussed more in Ref. [21], suggest that even smaller values of E_F, where $E_F < E_G$, may reproduce the measured D and $n^{\mathrm{exp}}_{2\mathrm{D}}$ values. Alternatively, we considered the case that the optical response arises from the bulk valence bands. Prior work has shown that the bulk valence band structure in the $(\mathrm{Bi,Sb})_2\mathrm{Te}_3$ system consists of a light hole band (LHB) and heavy hole band (HHB) [3,37,38]. The effective masses of the LHB and the HHB are $0.11m_e$ and $1.0m_e$ respectively, and the top of the HHB is approximately 30 meV below the LHB [37,38]. To recover the correct value of D for this sample, E_F would be 30 meV below the top of the LHB, However, this would yield an $n_{2\mathrm{D}}$ of 5×10^{12} cm^{-2}, over a factor of 2 smaller than what was measured.

Prior experiments have also pointed out that conventional SSs may coexist with the topologically protected SS of a TI [35]. Typically, the conventional SSs appear as a result of band bending, and are close in energy to the bulk bands, and contribute to the conductivity when $E_F \approx E_G$. Therefore, the large magnitude E_F required to access the conventional SSs, combined with their additional metallic response, would likely push D well above the limit imposed by f-sum rule analysis. It is therefore unlikely that our measured response has a significant component from the conventional SSs.

Further evidence of a dominant topological SS contribution to the response of the $(\mathrm{Bi,Sb})_2\mathrm{Te}_3$ system is identified in magnetoresistance measurements, plotted in the inset to Fig. 2. At low temperature, the magnetoresistance data show linear behavior with B, indicative of single band transport. Moreover, the figure reveals weak antilocalization in (symmetrized) magnetoresistance measurements (i.e., the cusp at the low-B field in the 2 K data), which has been thought to be a hallmark signature of topological SS transport [39]. However, theoretical work has shown that antilocalization may occur even in systems with bulk dominated transport, and therefore, antilocalization by itself, cannot be considered conclusive evidence for surface states [40]. Despite this stipulation, the magnetoresistance data, in conjunction with the low value of D revealed from optics, are consistent with low temperature transport that is dominated by topologically protected SSs.

The picture that emerges from the comparison of transport, optics, and previously measured photoemission is that the Dirac point is near the bottom of the conduction band, with E_F near the top of the valence band, as is illustrated in Fig. 1(b). Likewise, we illustrate the bulk band structure consisting of two hole bands offset from the Γ point, with an electron band at the Γ point, as measured previously [9,11,38]. The relative positioning of E_F, the Dirac point, and bulk bands that we propose has been observed in similar, albeit more highly doped, $(\mathrm{Bi}_{1-x}\mathrm{Sb}_x)_2\mathrm{Te}_3$ thin films [11]. Indeed, the distance from the Dirac point to the top of the valence band, as well as v_0 in this latter work, is consistent with our measurements. It is important to note that photoemission measurements of similarly doped samples often show that the Dirac point is below E_F [9], in contrast to our measurement of p-type carriers. This discrepancy can be understood in light of the aging effects, often observed TI systems, which generally shift the Dirac point downward relative to E_F. It is then likely that the capping layer of Se prevents the band bending, and the resulting accumulation layers, observed in other samples [35,36], yielding a response dominated by p-type SS carriers. Unfortunately, this same capping layer prevents direct verification of this hypothesis in our particular sample via photoemission.

The totality of our data clearly show that $(\mathrm{Bi,Sb})_2\mathrm{Te}_3$ alloys are a promising vehicle for advancing the field of TIs. In particular, the Drude oscillator strength lies at the threshold of the SS response upper bound, demonstrating the effectiveness of the alloy in reducing or eliminating bulk charge carriers. Furthermore, comparison of Drude parameters from optics to transport parameters from the Hall effect, coupled with weak antilocalization observed in low-temperature magnetotransport, shows consistency with surface transport with $v_0 \sim 4 \times 10^5$ m/s, in accord with angle resolved photoemission spectroscopy results [11]. Therefore, our data imply that $(\mathrm{Bi,Sb})_2\mathrm{Te}_3$ is an optimal candidate for isolating SS properties in further studies of keen interest, such as magneto-optical measurements [41–43] and electrostatic modification of SS charge carrier density in electric field effect devices [44–46].

Sample growth and characterization at Penn State was supported by DARPA (Grant No. N66001-11-1-4110), ONR (Grant No. N00014-12-1-0117), and ARO-MURI (Grants No. W911NF-12-1-0461) and No. ECS-0335765). Work at the University of California, San Diego (UCSD), on optical phenomena in vdW materials is supported by DOE-BES DE-FG02-00ER45799. DNB is funded by the Gordon and Betty Moore Foundation's EPiQS Initiative through Grant No. GBMF4533.

K. W. and B. C. contributed equally to this work.

*kwpost@physics.ucsd.edu

[1] M. Hasan and C. Kane, Rev. Mod. Phys. **82**, 3045 (2010).
[2] Y. Xia, D. Qian, D. Hsieh, L. Wray, A. Pal, H. Lin, A. Bansil, D. Grauer, Y. S. Hor, R. J. Cava *et al.*, Nat. Phys. **5**, 398 (2009).
[3] Y. L. Chen, J. G. Analytis, J.-H. Chu, Z. K. Liu, S.-K. Mo, X. L. Qi, H. J. Zhang, D. H. Lu, X. Dai, Z. Fang *et al.*, Science **325**, 178 (2009).

[4] D. Hsieh, Y. Xia, D. Qian, L. Wray, F. Meier, J. Dil, J. Osterwalder, L. Patthey, a. Fedorov, H. Lin *et al.*, Phys. Rev. Lett. **103**, 146401 (2009).

[5] S.-Y. Xu, M. Neupane, C. Liu, D. Zhang, A. Richardella, L. A. Wray, N. Alidoust, M. Leandersson, T. Balasubramanian, J. Sánchez-barriga *et al.*, Nat. Phys. **8**, 616 (2012).

[6] A. Hashibon and C. Elsässer, Phys. Rev. B **84**, 144117 (2011).

[7] B. C. Chapler, K. W. Post, A. R. Richardella, J. S. Lee, J. Tao, N. Samarth, and D. N. Basov, Phys. Rev. B **89**, 235308 (2014).

[8] Y. Jiang, Y. Y. Sun, M. Chen, Y. Wang, Z. Li, C. Song, K. He, L. Wang, X. Chen, Q.-K. Xue *et al.*, Phys. Rev. Lett. **108**, 066809 (2012).

[9] D. Kong, Y. Chen, J. J. Cha, Q. Zhang, J. G. Analytis, K. Lai, Z. Liu, S. S. Hong, K. J. Koski, S.-K. Mo *et al.*, Nat. Nanotechnol. **6**, 705 (2011).

[10] A. A. Reijnders, Y. Tian, L. J. Sandilands, G. Pohl, I. D. Kivlichan, S. Y. F. Zhao, S. Jia, M. E. Charles, R. J. Cava, N. Alidoust *et al.*, Phys. Rev. B **89**, 075138 (2014).

[11] J. Zhang, C.-Z. Chang, Z. Zhang, J. Wen, X. Feng, K. Li, M. Liu, K. He, L. Wang, X. Chen *et al.*, Nat. Commun. **2**, 574 (2011).

[12] L. Wu, M. Brahlek, R. Valdés Aguilar, A. V. Stier, C. M. Morris, Y. Lubashevsky, L. S. Bilbro, N. Bansal, S. Oh, and N. P. Armitage, Nat. Phys. **9**, 410 (2013).

[13] C. S. Tang, B. Xia, X. Zou, S. Chen, H.-W. Ou, L. Wang, a. Rusydi, J.-X. Zhu, and E. E. M. Chia, Sci. Rep. **3**, 3513 (2013).

[14] L. Wu, W.-K. Tse, M. Brahlek, C. Morris, R. Valdés Aguilar, N. Koirala, S. Oh, and N. Armitage, arXiv:1502.04577v1.

[15] It is unclear that optical transitions between SSs and bulk states are theoretically possible due to symmetry and spatial separation, but, moreover, such transitions cannot change the key result (3) relating the SS Drude oscillator strength to the Fermi level.

[16] Z. Li and J. P. Carbotte, Phys. Rev. B **87**, 155416 (2013).

[17] D. N. Basov, R. Averitt, D. van der Marel, M. Dressel, and K. Haule, Rev. Mod. Phys. **83**, 471 (2011).

[18] V. P. Gusynin, S. G. Sharapov, and J. P. Carbotte, Phys. Rev. B **75**, 165407 (2007).

[19] J. Sabio, J. Nilsson, and A. H. Castro Neto, Phys. Rev. B **78**, 075410 (2008).

[20] D. N. Basov, M. M. Fogler, a. Lanzara, F. Wang, and Y. Zhang, Rev. Mod. Phys. **86**, 959 (2014).

[21] See Supplemental Material at http://link.aps.org/supplemental/10.1103/PhysRevLett.115.116804 for details about discussions on optical conductivity in asymmetric bands SS bands, comparing D and n_{SS}, sample growth, the spectroscopic technique and corresponding models of the data, which includes Refs. [14,21–34].

[22] M. Dressel and G. Gruener, *Electrodynamics of Solids: Optical Properties of Electrons in Matter*, 1st ed. (Cambridge University Press, New York, 2002), Vol. 70.

[23] C.-X. Liu, X.-L. Qi, H. J. Zhang, X. Dai, Z. Fang, and S.-C. Zhang, Phys. Rev. B **82**, 045122 (2010).

[24] B. Wunsch, T. Stauber, F. Sols, and F. Guinea, New J. Phys. **8**, 318 (2006).

[25] C. Kittel, *Introduction to Solid State Physics,* 8th ed. (Wiley, New York, 2005).

[26] A. B. Kuzmenko, Rev. Sci. Instrum. **76**, 083108 (2005).

[27] R. D. Averitt and A. J. Taylor, J. Phys. Condens. Matter **14**, R1357 (2002).

[28] R. Yu, W. Zhang, H.-J. Zhang, S.-C. Zhang, X. Dai, and Z. Fang, Science **329**, 61 (2010).

[29] K. W. Post, Y. S. Lee, B. C. Chapler, A. A. Schafgans, M. Novak, A. A. Taskin, K. Segawa, M. D. Goldflam, H. T. Stinson, Y. Ando *et al.*, Phys. Rev. B **91**, 165202 (2015).

[30] R. Valdés Aguilar, A. V. Stier, W. Liu, L. S. Bilbro, D. K. George, N. Bansal, L. Wu, J. Cerne, a. G. Markelz, S. Oh *et al.*, Phys. Rev. Lett. **108**, 087403 (2012).

[31] H. Zhang, C.-X. Liu, X.-L. Qi, X. Dai, Z. Fang, and S.-C. Zhang, Nat. Phys. **5**, 438 (2009).

[32] D. Hsieh, Y. Xia, D. Qian, L. Wray, J. H. Dil, F. Meier, J. Osterwalder, L. Patthey, J. G. Checkelsky, N. P. Ong *et al.*, Nature (London) **460**, 1101 (2009).

[33] M. Neupane, S.-Y. Xu, L. A. Wray, A. Petersen, R. Shankar, N. Alidoust, C. Liu, a. Fedorov, H. Ji, J. M. Allred *et al.*, Phys. Rev. B **85**, 235406 (2012).

[34] T. Arakane, T. Sato, S. Souma, K. Kosaka, K. Nakayama, M. Komatsu, T. Takahashi, Z. Ren, K. Segawa, and Y. Ando, Nat. Commun. **3**, 636 (2012).

[35] M. S. Bahramy, P. D. C. King, A. de la Torre, J. Chang, M. Shi, L. Patthey, G. Balakrishnan, P. Hofmann, R. Arita, N. Nagaosa *et al.*, Nat. Commun. **3**, 1159 (2012).

[36] A. A. Taskin, Z. Ren, S. Sasaki, K. Segawa, and Y. Ando, Phys. Rev. Lett. **107**, 016801 (2011).

[37] V. A. Kulbachinskii, Z. M. Dashevskii, M. Inoue, M. Sasaki, H. Negishi, W. X. Gao, P. Lostak, J. Horak, and A. de Visser, Phys. Rev. B **52**, 10915 (1995).

[38] V. Kulbachinskii, V. Kytin, P. Tarasov, and N. Yuzeeva, Phys. Solid State **52**, 1830 (2010).

[39] L. Fu and C. L. Kane, Phys. Rev. B **76**, 045302 (2007).

[40] I. Garate and L. Glazman, Phys. Rev. B **86**, 035422 (2012).

[41] A. A. Schafgans, K. W. Post, A. A. Taskin, Y. Ando, X.-L. Qi, B. C. Chapler, and D. N. Basov, Phys. Rev. B **85**, 195440 (2012).

[42] W.-K. Tse and A. H. MacDonald, Phys. Rev. Lett. **105**, 057401 (2010).

[43] J. Maciejko, X.-L. Qi, H. D. Drew, and S.-C. Zhang, Phys. Rev. Lett. **105**, 166803 (2010).

[44] Z. Q. Li, E. A. Henriksen, Z. Jiang, Z. Hao, M. C. Martin, P. Kim, H. L. Stormer, and D. N. Basov, Nat. Phys. **4**, 532 (2008).

[45] J. Horng, C.-F. Chen, B. Geng, C. Girit, Y. Zhang, Z. Hao, H. a. Bechtel, M. Martin, A. Zettl, M. F. Crommie *et al.*, Phys. Rev. B **83**, 165113 (2011).

[46] G. S. Jenkins, D. C. Schmadel, A. B. Sushkov, H. D. Drew, M. Bichler, G. Koblmueller, M. Brahlek, N. Bansal, and S. Oh, Phys. Rev. B **87**, 155126 (2013).

Supplemental Materials: Sum rule constraints on the surface state conductance of topological insulators

K.W. Post,[1,*], B.C. Chapler,[1] M.K. Liu,[1] J.S. Wu,[1] H.T. Stinson,[1] M.D. Goldflam,[1] A.R. Richardella,[2] J.S. Lee,[2] A.A. Reijnders,[3], K.S. Burch,[4] M.M. Fogler,[1], N. Samarth,[2], and D.N. Basov[1]

[1]*Physics Department, University of California-San Diego, La Jolla, California 92093, USA*

[2]*Department of Physics, the Pennsylvania State University, University Park, Pennsylvania 16802, USA*

[3]*Department of Physics and Institute for Optical Sciences, University of Toronto, Toronto, Ontario M5S 1A7, Canada*

[4]*Department of Physics, Boston College, Chestnut Hill, Massachusetts 02467, USA*

(Dated: July 29, 2015)

I. OPTICAL CONDUCTIVITY OF SURFACE STATES

Optical conductivity in Dirac like systems, when E_F is at the Dirac point, arises from interband transitions, as illustrated in Fig. 1 of the main text. The standard Kubo formalism for calculating optical conductivity is given by [1]:

$$\sigma_1(\omega, \vec{q}) = \frac{1}{4\pi\omega} \int |\langle s| \hat{j}_x |s'\rangle|^2 \delta(\hbar\omega - \hbar\omega_{s,s'}) d\vec{k} \tag{S1}$$

$$\hat{j}_x = ev\sigma_x \tag{S2}$$

where s and s' are the final and initial states, respectively, $\omega_{s,s'}$, is the difference in energy between the initial and final states, and $\hat{j}_x$ is the current operator. Importantly, $\langle s| \hat{j}_x |s'\rangle$ is related to the derivative of the overlap between s and s', with respect to energy. For the case of our modeled topological insulator (TI) system, the hexagonal warping and non-linearity increases the rate at which s and s' change as a function of momentum, therefore increasing the overlap of $\langle s| \hat{j}_x |s'\rangle$, and the corresponding conductivity at higher wavenumbers.

Within the framework of Kubo formalism, and taking into account the spin and momentum locking in TIs [2], we calculated the optical conductivity, assuming a surface state dispersion of:

$$E(k, \theta) = \beta k^2 \pm \sqrt{v_0^2 k^2 + \lambda^2 k^6 \cos^3(3\theta)}. \tag{S3}$$

The parameters β and v_0 are the quadratic and linear component of the dispersion, respectively, while λ is related to the hexagonal warping. Eqn. S3 is similar to that used in [3], with the addition of a quadratic correction. Utilizing the relationship between momentum and spin of SS carriers [2], the wavefunction of the SS charge carriers can be determined and evaluated in the Kubo framework, described by Eqn. S1. Moreover, when E_F is at the Dirac point ($E_F = 0$), interband transitions are allowed at all energies. The resulting conductivity is then given by:

$$\sigma_1(\omega) = \frac{e^2}{32\hbar\pi\omega^2} \int_0^{2\pi} v_0^2 k^2 \frac{\omega^2/4 - 2\lambda^2 k^6 \cos^3(3\theta) + 9\lambda^2 k^6}{\omega^2/4 + 2\lambda^2 k^6 \cos^3(3\theta)} d\theta, \tag{S4}$$

where k is a function of θ, and is obtained by solving the equation

$$v_0^2 k^2 + \lambda^2 k^6 \cos^3(3\theta) = \frac{\omega^2}{4}. \tag{S5}$$

A closed form of $\sigma_1(\omega)$ can then be obtained by expanding about small λ. This derivation was guided in large part by prior theoretical work on the optical response of Dirac electron systems [3–5].

II. EXTENDED SUM RULE ANALYSIS OF SURFACE STATES

The modifications to the optical conductance described in the previous section are useful for extending the sum rule constraint, described in the main text, to systems characterized by hexagonal warping and band asymmetry. Accordingly, we have considered the optical conductance arising from three different SS dispersions, shown in Fig. S1a, S1b and S1c. The dispersion shown in Fig. S1a is the same as that used in the main text for establishing the sum rules. In Fig. S1b, the dispersion is modified to include minor hexagonal warping, and a smaller v_0. Lastly, in Fig. S1c, we show the surface state dispersion of an n-type $(Bi_{0.5}Sb_{0.5})_2Te_3$ crystal, extracted from photoemission data in [6], which was characterized by significant hexagonal warping and band asymmetry. Although not comprehensive, examining these dispersions and their corresponding optical response may provide some intuition as to how features of the SS dispersion influence the optical conductance.

In these schematics, we have also indicated the bulk band dispersion with the blue dotted lines. The bulk band structure we show is based on combined photoemission and transport [6–8]. These data indicate the presence of a light and heavy hole band that are both offset from the Γ-point, and an electron band centered in the Brillouin zone. The relative positioning of E_F, the Dirac point, and the bulk bands in Fig. S1a and S1b illustrate scenarios consistent with our experimental observation of p-type carriers. The alternative n-type picture that was measured in [6] is illustrated in Fig. S1c.

The conductance spectra, calculated when $E_F = 0$, corresponding to the SS dispersions shown in Fig. S1a,S1b and S1c are plotted as the dotted line in Fig. S1d, S1e and S1f, respectively. However, the schematic shown in Fig. S1a-c shows E_F shifted away from the Dirac point, yielding a system where hole (electron) states are depopulated

(populated), as in Fig. S1a and S1b (Fig. S1c). For interband transitions to occur in these systems, it must be possible to excite an electron from a populated hole state, to a depopulated electron state, while conserving momentum ($\vec{k}$). Thus, the populated or depopulated states block interband transitions below a threshold energy (ω_{th}). For symmetric bands, $\omega_{th} = 2|E_F|$. In an asymmetric SS dispersion, ω_{th} must be determined on a case by case basis. The blocked interband transitions below ω_{th} suppresses the optical conductance. However, the f-sum rule, described in the main text demands that spectral weight cannot be lost, but is instead transferred into the Drude oscillator. The conductance spectra corresponding to the schematics in Fig. S1a-c, where $|E_|F = E_g$, are indicated by the solid lines in Fig. S1d-f, respectively.

A salient feature in these conductance spectra is that increasing the hexagonal warping, increases the upturn in Conductance as ω increases. Accordingly, a higher hexagonal warping corresponds to a larger area of suppressed spectral weight, resulting in a larger Drude spectral weight (D), which is indicated in Fig. S1d-f. In addition, for comparison with our experimental data, we can extract the SS carrier density (n_{SS}) from the extracted SS dispersion via:

$$n_{SS} = \frac{1}{8\pi^2}\int_0^{2\pi} k_F^2(\theta)d\theta.$$

Since we are probing two surfaces, the total two dimensional carrier density (n_{2D}) is given by $n_{2D} = 2 \cdot n_{SS}$, and is indicated in Fig. S1d-f. The experimentally obtained values were $D^{exp} = 0.13meV$ and $n_{2D}^{exp} = 1.3 \times 10^{13} cm^{-2}$. The schematic shown in Fig. S1a predicts D and n_{2D} values that closely match what was measured, however, for an exact match E_F would have to be within the bulk valence band. In contrast, slight modifications to the SS dispersion as in Fig. S1b overestimates the values of D and n_{2D} when $|E_F| = E_G$. Instead, our experimental values are reproduced when $|E_F| = 0.19eV$, a value smaller than E_G, suggesting our measurements are consistent with a completely surface dominated response, without bulk contributions. Interestingly, the n-type schematic shown in Fig. S1c corresponds to a D even larger than what we measured, but significantly underestimates n_{2D}, due to the reduced area of the Fermi surface. Thus, this picture is inconsistent with our measurements.

III. COMPARISON OF D AND n_{2D} FOR LINEAR SS BANDS

In the main text, our analysis of D and n_{2D}, implied an $|E_F|$ of 221 meV, thereby suggesting E_F resides 16 meV in the bulk valence band (BVB). However, this estimate is incomplete since it neglects contributions to D and n_{2D} from the bulk bands, which are significant when E_F is at the edge of the (BVB). To illustrate this latter effect, we have seperately calculated D and n_{2D}, as a function of E_F for the three elements comprising the composite system: SS bands, the light hole band (LHB), and the heavy hole band (HHB). The effective masses of the LHB and the HHB, as well as their relative position, were taken from [7, 8] and used to assemble the schematic band structure shown in Fig. S2a. To calculate D and n_{2D} from this schematic band structure, we utilized the well known relationships between m^*, E_F, n_{2D} and D for bulk bands [9–11], and the analagous relationships for linear bands detailed in the main text. The resulting E_F dependent values of D and n_{2D} are plotted in Fig. S2b and S2c, respectively. The black, red, and green lines indicate the individual contribution from the SS, the LHB and the HHB, respectively. The value of D or n_{2D} that we would expect to measure is the sum of these these latter three contributions, which is indicated by the dotted gray line. Lastly, the blue line indicates our experimentally obtained value. Therefore, a more realistic value of E_F, where the combined bulk and surface contributions are taken into account corresponds to the point where the dotted gray line intersects the blue line. In the case of the D, the intersection occurs at E_F=211 meV, which is only 5 meV into the LHB. The total carrier density corresponding to this value E_F is $1.16\times10^{13}\text{cm}^{-2}$, in close agreement with our experimentally measured value of $1.28 \times 10^{13}\text{cm}^{-2}$. Moreover, the surface carriers in this scenario account for approximately 98% of the total carriers, suggesting a highly surface dominated response.

Alternatively, we considered the possibility that the carriers we measure arise solely from the bulk bands, where the resulting E_F dependent D and n_{2D} spectra are plotted in Fig. S2d and S2e, respectively. Again, the red and green lines indicate the contributions from the LHB and the HHB, and the sum of these two bulk contributions is the dotted gray line. In these plots, the dotted gray line intersects the measured D at $E_F = 30\text{meV}$. However, this value of E_F would imply an n_{2D} of $5 \times 10^{12}\text{cm}^{-2}$, less than half of what was measured. In fact, it was found that neither of the bulk valence bands, in isolation, could consistently reproduce our measured D and n_{2D} values. Even so, it was possible to adjust the relative positioning of these bands could produce a multi-band response that matches our measurements. However, such a multi-band system would contradict the linear behavior of the Hall resistance, discussed in the main text, which indicates a single carrier species. This analysis emphasizes the notion that our data can be consistently described by assuming a SS dominated response, but not bulk.

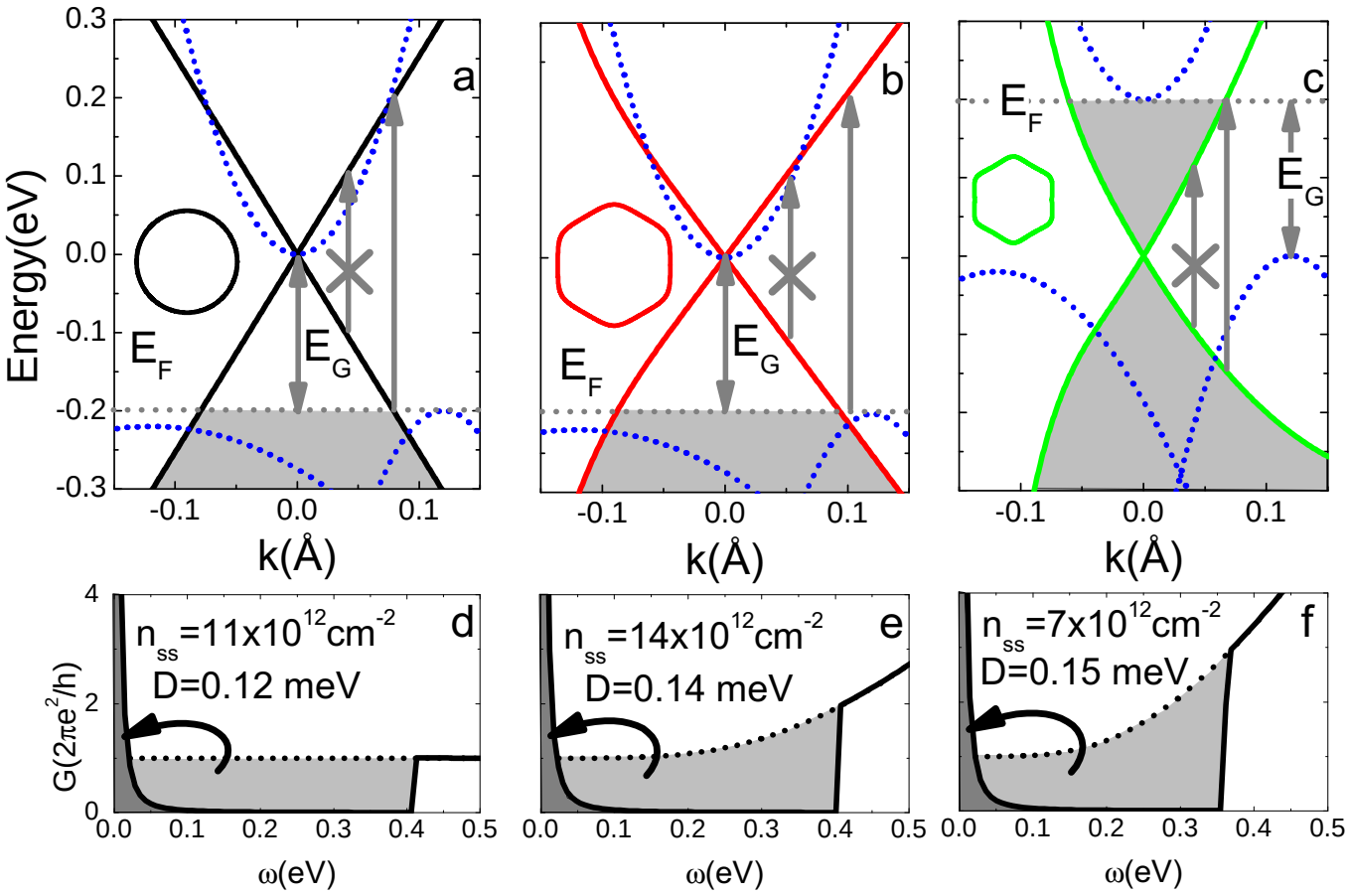

FIG. S1. Panels (a), (b) and (c) schematically show the SS dispersion and bulk band structure corresponding to different experimental scenarios. (a) shows a SS dispersion without hexagonal warping, where the Dirac point is at the bottom of the bulk conduction band. (b) shows a dispersion similar to (a), with the addition of minor hexagonal warping and a slightly smaller v_0. (c) shows the SS dispersion, extracted from [6], where the Dirac point as at the same energy as the bulk valence band, and E_F is at the bottom of the bulk conduction band. The optical conductance corresponding to each of the schematics (a), (b) and (c), are shown in (d), (e) and (f), respectively. In (d),(e) and (f), the dotted line shows the predicted conductance when E_F is at the Dirac point, whereas the solid line indicates the conductance expected when $|E_F| = E_G$, as indicated in the corresponding schematics.

IV. DRUDE-LORENTZ FITTING OF THE CONDUCTANCE SPECTRA

In the main text, only the Drude-Lorentz fitting of the 8K conductance data was shown. The same fitting procedure was employed to extracte the value of D and scattering time τ for all data sets that are shown in Fig. 2c and 2d of the main text. For completeness, the Drude-Lorentz fits to the conductance spectra at all measured temperatures are shown in Fig. S3

The most prominent features of these spectra are the two phonons at 6 meV and 8 meV. The lower energy resonance has a center frequency in close agreement with the E_u^1 phonon mode of Bi_2Te_3 [12], while the weaker higher energy mode has two possibilities. The center frequency of this latter mode suggests assignment to either the E_u^1 mode of Sb_2Te_3, or the A_{1g}^1 mode, which is at similar energies in both stoichiometric compounds [12]. The A_{1g}^1 mode is typically only Raman active, however, this mode may become IR active in the $(Bi,Sb)_2Te_3$ alloy due to the broken translational symmetry introduced via Bi:Sb substitution.

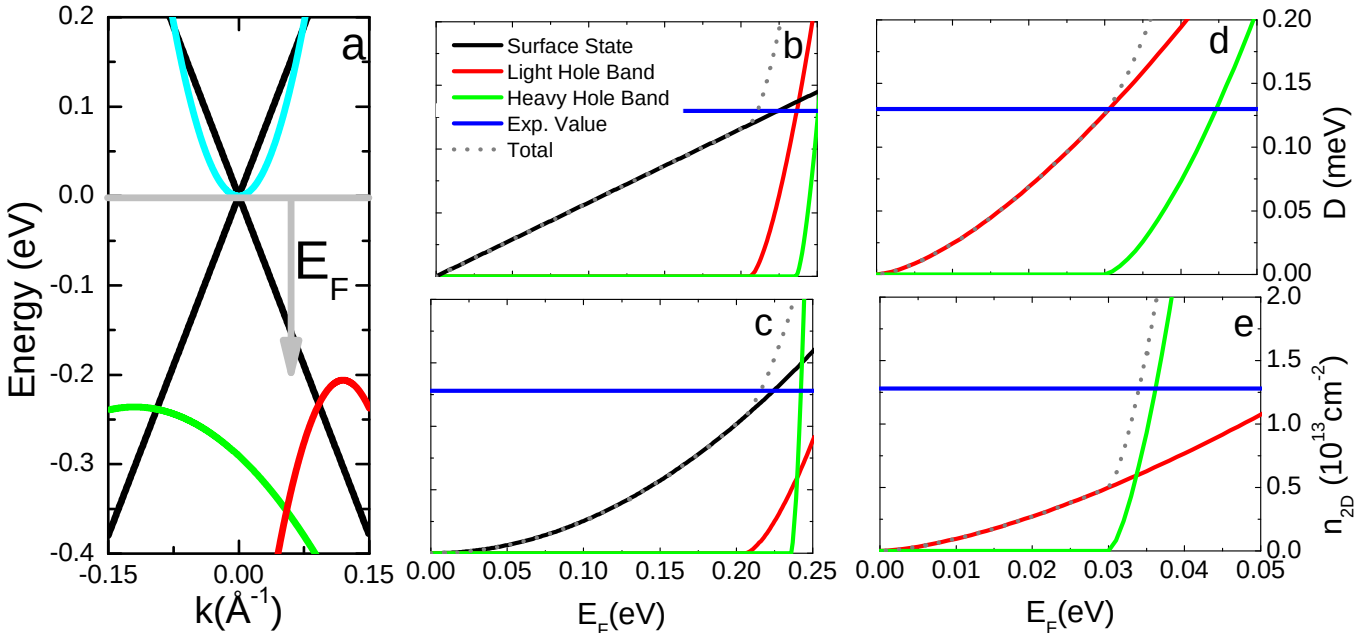

FIG. S2. A schematic band structure of the measured $(Bi,Sb)_2Te_3$ thin film is shown in (a). The surface state band, the conduction band, the light hole band and the heavy hole band are indicated by the black, cyan, red and green lines, respectively. The E_F dependent values of D and n_{2D} that would be expected to arise from the composite bulk and surface response of this system are plotted in (b) and (c), respectively. In (b) and (c), E_F is defined relative to the Dirac point. Alternatively, the E_F dependent D and n_{2D} that would be expected in the absence of the SSs are plotted in (d) and (e), respectively. In these latter two panels, E_F is defined relative to the top of the light hole band. In panels (b-e) the blue line indicates the experimentally measured value, while the black, red and green lines indicate the isolated contribution to the D or n_{2D} spectra from the SS, the light hole band and the heavy hole band respectively while the dotted gray line indicates the sum of these latter three contributions, and the value that we would expect to measure.

V. SAMPLE GROWTH

The $(Bi,Sb)_2Te_3$ films in this study were prepared using molecular beam epitaxy, with a composition of approximately 54% Sb to 46% Bi. These films were grown along the c-axis with a thicknes of 58nm on an insulating InP (111) substrate, where the InP oxide was desorbed under a flux of As to retain a smooth surface for the TI growth. Our films were grown under a Te overpressure, with a Te/(Bi+Sb) beam equivalent pressure ratio of about 7. These growth conditions were determined to yield samples that could be gated through the Dirac point, and possessed insulating resistance vs. temperature curves. The film was capped with a 10nm insulating amorphous Se layer at room temperature, which prevents oxidation and has negligible effects on low energy optical spectroscopy measurements, as demonstrated in [13]. We confirmed the opticaly inert nature of the Se capping layer by also measuring an InP substrate with a thin layer of Se, and comparing it to bare InP. Further characterization of the film was done using x-ray diffraction, and low temperature magneto-transport. Likewise, the film thickness was determined by X-ray reflectivity, and the composition by secondary ion mass spectroscopy measurements on similar samples.

VI. SPECTROSCOPIC TECHNIQUE

The energy range covered by the Terahertz-Time domain spectroscopy (THz-TDS) and fourier transform infrared (FTIR) experiments are roughly 2-10 and 5-900 meV, respectively. The complex, frequency dependent optical constants of the film ($\tilde{\epsilon}(\omega)$,$\tilde{n}(\omega)$,$\tilde{\sigma}(\omega)$, which are all algebraically related [1]), were determined seperately for the THz-TDS and FTIR experiments, and then merged together. To obtain the optical constant of the film for this two layer system (film+substrate), it was necessary to first precisely determine the optical constants of the InP substrate at each temperature. For the FTIR data, we constructed a multi-layer, multi-oscillator, Kramers-Krònig consistet model fit of the raw transimssion data, yielding the optical constants of the film [14]. In the THz-TDS experiment, we measure

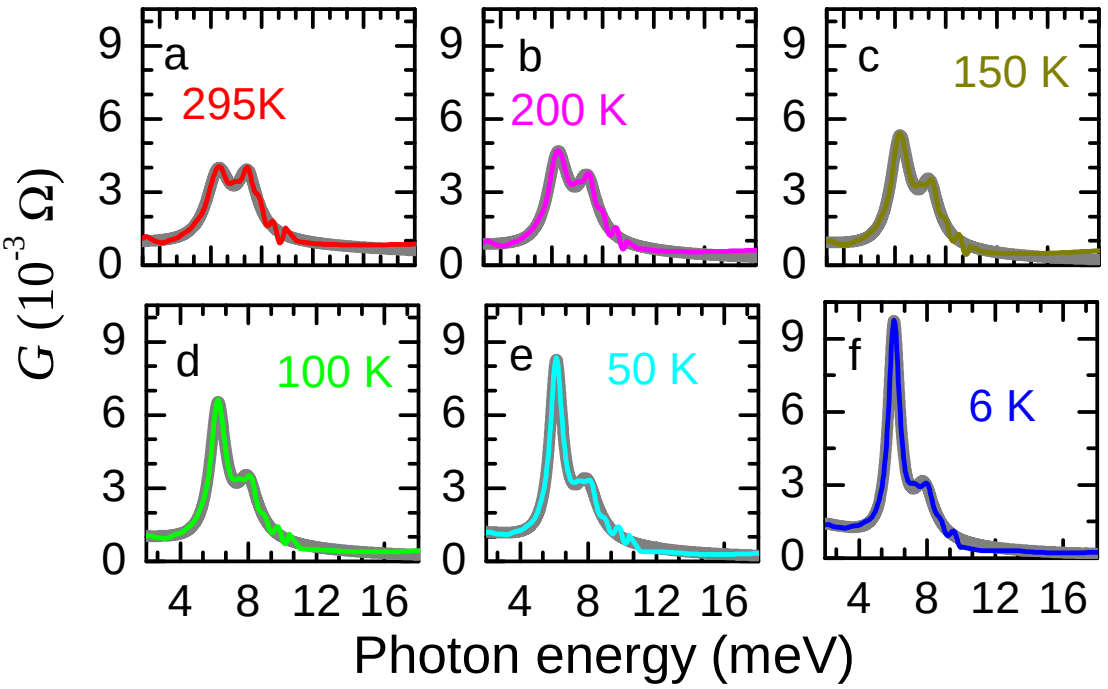

FIG. S3. The experimental conductance spectra of $(Bi,Sb)_2Te_3$ (colored lines) are shown for all measured temperatures, along with the Drude-Lorentz fit (gray lines).

the time-resolved transmitted electric field, from which the optical constants are calculated directly [15].

VII. ENERGY GAP

Establishing the maximum Drude spectral weight required a value for E_G, which can be readily determined from our data. In Fig. S4a we plot $(\epsilon_2(\omega))^2$ from 75-900 meV, where $\epsilon_2(\omega)$ is the imaginary part of the complex, frequency dependent dielectric function, $\tilde{\epsilon}(\omega) = \epsilon_1(\omega) + i\epsilon_2(\omega)$. E_G is found from the x-intercept of a linear fit to $(\epsilon_2(\omega))^2$ in the linear onset regime, $\simeq 200 - 250$ meV [16]. The resulting value of E_G is plotted as a function of temperature in Fig. S4b. The data show a relatively temperature independent E_G of 206.5±3.4 meV, in contrast to the significant temperature dependence of E_G observed in other works [17]. Also noticeable in the $(\epsilon_2(\omega))^2$ spectra are distinct resonant features at $\omega > E_G$, which are suggestive of Van Hove singularities in the $(Bi,Sb)_2Te_3$ band structure, but are not discussed in detail in this work [16].

VIII. THREE LAYER MODEL OF THE TI SYSTEM

Our method of extracting the optical constants, and thus D, are consisten with silimar analysis in the literature [13, 18, 19]. However, an assertion of SS conductance requires a 3-layer model for the TI film, *i.e.* two conductive surfaces and one insulating bulk layer, whereas in the main text, the value of D is extracted using a model consisting of one layer and a single Drude, where a single layer accounts for the effect of both surfaces. Thus, to confirm the plausibility that theDrude conductance is due to SS electrons, the THz-TDS transmission was alternatively modeled assuming 3-layers + substrate: (1) 1 nm surface layer, (2) 58 nm bulk layer, (3) 1 nm surface layer, and (4) 0.5 mm InP substrate, as illustrated schematically in Fig. S5. The Se capping layer was neglected since, as stated earlier, it was found to have a negligible effect on the optical response of the system. We ascribe single (identical) Drude oscillators to layers (1) and (3), with the bulk layer (2) having two lorentzian oscillators to describe the phonons. The choice of 1nm for the surface layers is based on theoretical predictions [20], though the choice in SS thickness

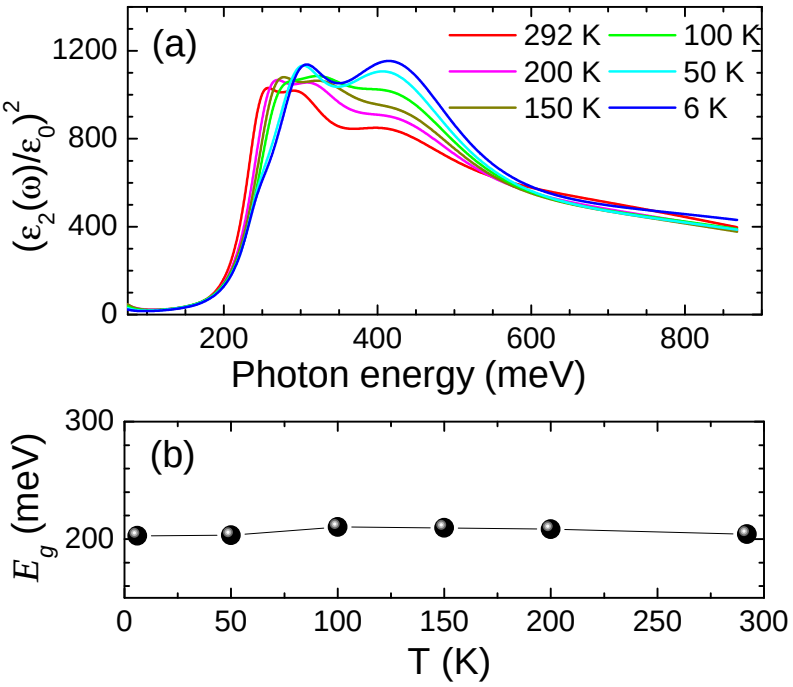

FIG. S4. Panel (a) shows the $(\epsilon_2/\epsilon_0)^2$ spectra at all measured temperatures, where the lienar region near 200 meV indicates the onset of interband transitions. The magnitude of E_G is extracted from these spectra using a linear fit to $(\epsilon_2/\epsilon_0)^2$ where teh x-axis intercept corresponds to the value of E_G. E_G extracted using this procedure is plotted as a function of temperature in (b).

has negligible effect, as long as it is much less than the optical penetration depth [21]. Under this 3-layer modeling, the D extracted for each surface of the 6K THz-TDS transmission is 0.07 meV, for a total (D^s_{3layer}) of 0.14 meV. This is in good agreement with D=0.13 meV extracted from the conductance that was calculated directly from the THz-TDS data. The agreement between these two methods, and the proximity to the threshold of D^s_{max}, confirms the plausibility that the Drude conductance observed is dombinated by the topological SSs.

IX. BOLTZMANN DERIVATION OF THE DRUDE SPECTRAL WEIGHT

The f-sum rule analysis, detailed in the main text, offers an intuitive way to understand limits on the Drude spectral weight in Dirac systems. However, the value of D can be alternatively derived using the Boltzmann equation, which requires only that the shape of the Fermi surface is known, rather than the entire band structure. With this knowledge of the Fermi surface, σ_{xx} is given by the Boltzmann equation:

$$\sigma_{xx} = \frac{e^2}{i\omega - 1/\tau} \int v_x^2 \frac{k_F}{|\partial E/\partial k|} d\phi \tag{S6}$$

where D is given by:

$$D = e^2 \int v_x^2 \frac{k_F}{|\partial E/\partial k|} d\phi. \tag{S7}$$

With this equation, D can be calculated simply from the SS dispersion, given by Eqn. S3. We therefore extracted the SS dispersion of a number of TI systems from photoemission data, which are shown in Fig. S6b, with the corresponding Fermi surface at $E_F = E_G$ shown in Fig. S6c. The resulting values of D are plotted as a function of E_F in Fig. S6c, with the energy gap of the different materials indicated by the arrows, colored to match their respective system. Using the same reasoning as in the main text, the estimated maximum value of D without bulk contributions is achieved when $E_F = E_G$. The maximum values of D obtained from the Boltzmann derivation ($D^s_{Boltz,max}$) are shown next to the experimentally obtained values of D in Table I, a modified verion of the table shown in the text. The results of this complementary analysis of D are consistent with our previous conclusions.

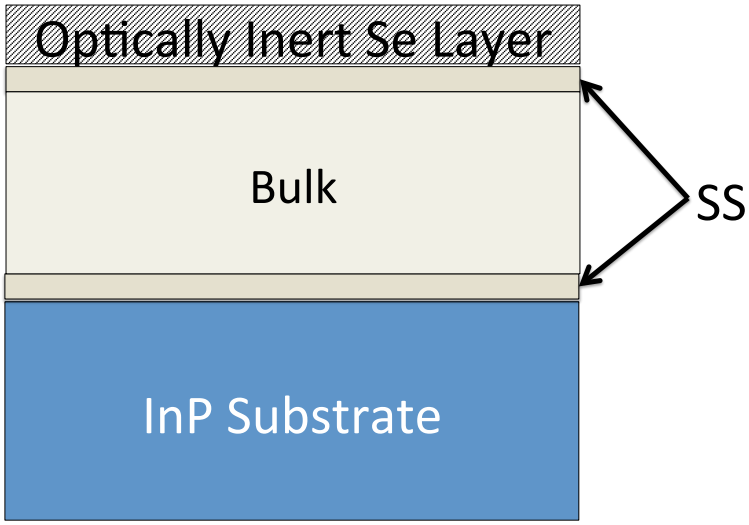

FIG. S5. A schematic of the 3 layer BST+Substrate model that was used for extracting D. The top Se capping layer is optically inert, and was thus not considered in the model. The BST SS layers consisted ofa single Drude oscillator, with identical values of D and τ. The model for the BST bulk included only two lorentzian oscillators to capture the phonon modes. The InP substrate was measured and characterized separately, without the BST system.

TABLE I. Bulk band gap E_g, experimental Drude oscillator strength D^{exp} from transmission based experiments, modeled Drude oscillator strength D^s_{3layer} where conductance is assumed to be from 2 topological surfaces with an insulating bulk, and theoretical upper bound of the Drude oscillator strength $D^s_{\text{Boltz,max}}$ of prototypical strong TIs obtained using the bulk energy gap, and the SS dispersion shown in Fig. S6a. Values of D are all taken from low-temperature data (6–20 K). All units are meV. †The results of Ref.[21] are from reflection based experiments, and thus only one topological surface is considered.

TI material	E_g	D^{exp}	D^s_{3layer}	$D^s_{\text{Boltz,max}}$	Refs.
Bi_2Se_3	300	0.09–0.70	–	0.17	[13, 18, 24, 27]
Bi_2Te_3	142	1.26	–	0.09	[10]
$Bi_{1.5}Sb_{0.5}Te_{1.8}Se_{1.2}$	340	1.42	–	0.34	[19]
Bi_2Te_2Se†	290	–	0.83	0.14	[21]
$Bi_{0.92}Sb_{1.08}Te_3$	207	0.13	0.14	0.15	This work

[1] M. Dressel and G. Gruener, *Electrodynamics of Solids: Optical Properties of Electrons in Matter*, vol. 70 (Cambridge University Press, New York, New York, USA, 2002), 1st ed., ISBN 0 511 01439 2.

[2] C.-X. Liu, X.-L. Qi, H. J. Zhang, X. Dai, Z. Fang, and S.-C. Zhang, Phys. Rev. B **82**, 045122 (2010), URL `http://link.aps.org/doi/10.1103/PhysRevB.82.045122`.

[3] Z. Li and J. P. Carbotte, Physical Review B **87**, 155416 (2013), ISSN 1098-0121, URL `http://link.aps.org/doi/10.1103/PhysRevB.87.155416`.

[4] B. Wunsch, T. Stauber, F. Sols, and F. Guinea, New Journal of Physics **8**, 318 (2006), ISSN 1367-2630, URL `http://stacks.iop.org/1367-2630/8/i=12/a=318?key=crossref.1ac84bfc3f85e7367b9a281336c35735`.

[5] L. Fu, Physical Review Letters **103**, 266801 (2009), ISSN 0031-9007, URL `http://link.aps.org/doi/10.1103/PhysRevLett.103.266801`.

[6] D. Kong, Y. Chen, J. J. Cha, Q. Zhang, J. G. Analytis, K. Lai, Z. Liu, S. S. Hong, K. J. Koski, S.-K. Mo, et al., Nature nanotechnology **6**, 705 (2011), ISSN 1748-3395, URL `http://www.ncbi.nlm.nih.gov/pubmed/21963714`.

[7] V. Kulbachinskii, V. Kytin, P. Tarasov, and N. Yuzeeva, Physics of the Solid State **52**, 1830 (2010).

[8] V. Kulbachinskii, Z. Dashevskii, M. Inoue, M. Sasaki, H. Negishi, W. Gao, P. Lostak, J. Horak, and A. de Visser, Phys. Rev. B **52**, 10915 (1995).

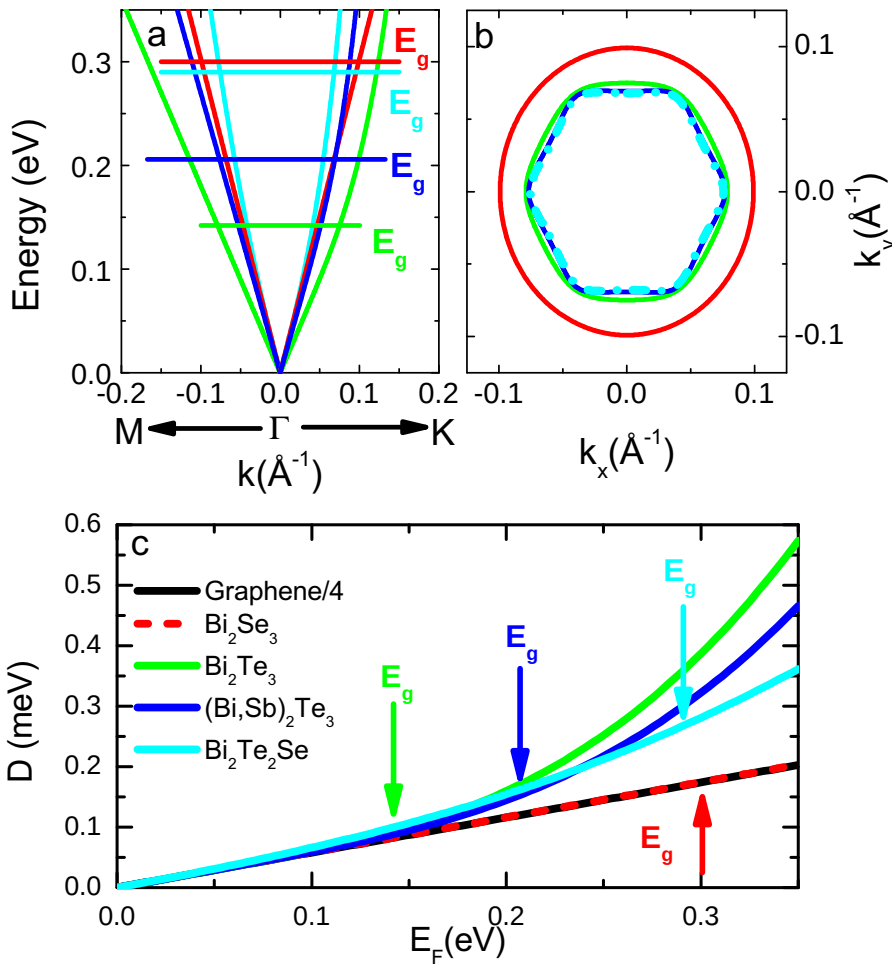

FIG. S6. The SS dispersion above the Dirac point, which was extracted from photoemission data [6, 22–26], is shown in (a) for four different TI systems. The lines, colored to match their respective system, indicate the bulk energy gap, with the Fermi surface corresponding to $E_F = E_G$ plotted in (b). The value of D, extracted from the SS dispersion using Eqn. S7, is plotted as a function of E_F in (c), with the bulk energy gap indicated by the arrows, colored to match their respective system.

[9] D. N. Basov, R. D. Averitt, D. van der Marel, M. Dressel, K. Haule, and C. Gene, Reviews of Modern Physics **83**, 471 (2011), ISSN 0034-6861, URL http://link.aps.org/doi/10.1103/RevModPhys.83.471.

[10] B. C. Chapler, K. W. Post, a. R. Richardella, J. S. Lee, J. Tao, N. Samarth, and D. N. Basov, Physical Review B **89**, 1Fr (2014), ISSN 1550235X, 1405.4916.

[11] C. Kittel, *Introduction to Solid State Physics* (2005), 8th ed.

[12] W. Richter, H. Kohler, and C. Becker, Phys. Stat. Sol. (b) **84**, 619 (1977).

[13] L. Wu, M. Brahlek, R. Valdés Aguilar, a. V. Stier, C. M. Morris, Y. Lubashevsky, L. S. Bilbro, N. Bansal, S. Oh, and N. P. Armitage, Nature Physics pp. 1–5 (2013), ISSN 1745-2473, URL http://www.nature.com/doifinder/10.1038/nphys2647.

[14] A. B. Kuzmenko, Review of Scientific Instruments **76**, 083108 (2005), ISSN 00346748, URL http://link.aip.org/link/RSINAK/v76/i8/p083108/s1&Agg=doi.

[15] R. D. Averitt and A. J. Taylor, Journal of Physics: Condensed Matter **14**, R1357 (2002).

[16] R. Yu, W. Zhang, H.-J. Zhang, S.-C. Zhang, X. Dai, and Z. Fang, Science (New York, N.Y.) **329**, 61 (2010), ISSN 1095-9203, URL http://www.ncbi.nlm.nih.gov/pubmed/20522741.

[17] K. W. Post, Y. S. Lee, B. C. Chapler, A. A. Schafgans, M. Novak, A. A. Taskin, K. Segawa, M. D. Goldflam, H. T. Stinson, Y. Ando, et al., Phys. Rev. B **91**, 165202 (2015), URL http://link.aps.org/doi/10.1103/PhysRevB.91.165202.

[18] R. Valdés Aguilar, a. V. Stier, W. Liu, L. S. Bilbro, D. K. George, N. Bansal, L. Wu, J. Cerne, a. G. Markelz, S. Oh, et al., Physical Review Letters **108**, 087403 (2012), ISSN 0031-9007, URL http://link.aps.org/doi/10.1103/PhysRevLett.108.087403.

[19] C. S. Tang, B. Xia, X. Zou, S. Chen, H.-W. Ou, L. Wang, a. Rusydi, J.-X. Zhu, and E. E. M. Chia, Scientific reports **3**, 3513 (2013), ISSN 2045-2322, URL http://www.pubmedcentral.nih.gov/articlerender.fcgi?artid=3865466&tool=pmcentrez&rendertype=abstract.

[20] H. Zhang, C.-X. Liu, X.-L. Qi, X. Dai, Z. Fang, and S.-C. Zhang, Nature Physics **5**, 438 (2009), ISSN 1745-2473, URL http://www.nature.com/doifinder/10.1038/nphys1270.

[21] A. A. Reijnders, Y. Tian, L. J. Sandilands, G. Pohl, I. D. Kivlichan, S. Y. F. Zhao, S. Jia, M. E. Charles, R. J. Cava, N. Alidoust, et al., Physical Review B **89**, 075138 (2014), ISSN 1098-0121, URL http://link.aps.org/doi/10.1103/PhysRevB.89.075138.

[22] D. Hsieh, Y. Xia, D. Qian, L. Wray, J. H. Dil, F. Meier, J. Osterwalder, L. Patthey, J. G. Checkelsky, N. P. Ong, et al., Nature **460**, 1101 (2009), ISSN 1476-4687, URL http://www.ncbi.nlm.nih.gov/pubmed/19620959.

[23] M. Neupane, S.-Y. Xu, L. A. Wray, A. Petersen, R. Shankar, N. Alidoust, C. Liu, A. Fedorov, H. Ji, J. M. Allred, et al., Physical Review B **85**, 235406 (2012), ISSN 1098-0121, URL http://link.aps.org/doi/10.1103/PhysRevB.85.235406.

[24] Y. Xia, D. Qian, D. Hsieh, L. Wray, A. Pal, H. Lin, A. Bansil, D. Grauer, Y. S. Hor, R. J. Cava, et al., Nature Physics **5**, 398 (2009), ISSN 1745-2473, URL http://www.nature.com/doifinder/10.1038/nphys1274.

[25] Y. L. Chen, J. G. Analytis, J.-H. Chu, Z. K. Liu, S.-K. Mo, X. L. Qi, H. J. Zhang, D. H. Lu, X. Dai, Z. Fang, et al., Science (New York, N.Y.) **325**, 178 (2009), ISSN 1095-9203, URL http://www.ncbi.nlm.nih.gov/pubmed/19520912.

[26] T. Arakane, T. Sato, S. Souma, K. Kosaka, K. Nakayama, M. Komatsu, T. Takahashi, Z. Ren, K. Segawa, and Y. Ando, Nature communications **3**, 636 (2012), ISSN 2041-1723, URL http://www.ncbi.nlm.nih.gov/pubmed/22273674.

[27] L. Wu, W.-K. Tse, M. Brahlek, C. Morris, R. Valdés Aguilar, N. Koirala, S. Oh, and N. Armitage (2015), 1502.04577v1.

Supplemental Materials: Sum rule constraints on the surface state conductance of topological insulators

K.W. Post,[1,*], B.C. Chapler,[1] M.K. Liu,[1] J.S. Wu,[1] H.T. Stinson,[1] M.D. Goldflam,[1] A.R. Richardella,[2] J.S. Lee,[2] A.A. Reijnders,[3], K.S. Burch,[4] M.M. Fogler,[1], N. Samarth,[2], and D.N. Basov[1]

[1]*Physics Department, University of California-San Diego, La Jolla, California 92093, USA*

[2]*Department of Physics, the Pennsylvania State University, University Park, Pennsylvania 16802, USA*

[3]*Department of Physics and Institute for Optical Sciences, University of Toronto, Toronto, Ontario M5S 1A7, Canada*

[4]*Department of Physics, Boston College, Chestnut Hill, Massachusetts 02467, USA*

(Dated: July 29, 2015)

I. OPTICAL CONDUCTIVITY OF SURFACE STATES

Optical conductivity in Dirac like systems, when E_F is at the Dirac point, arises from interband transitions, as illustrated in Fig. 1 of the main text. The standard Kubo formalism for calculating optical conductivity is given by [1]:

$$\sigma_1(\omega, \vec{q}) = \frac{1}{4\pi\omega} \int |\langle s| \hat{j}_x |s'\rangle|^2 \delta(\hbar\omega - \hbar\omega_{s,s'}) d\vec{k} \tag{S1}$$

$$\hat{j}_x = ev\sigma_x \tag{S2}$$

where s and s' are the final and initial states, respectively, $\omega_{s,s'}$, is the difference in energy between the initial and final states, and $\hat{j}_x$ is the current operator. Importantly, $\langle s| \hat{j}_x |s'\rangle$ is related to the derivative of the overlap between s and s', with respect to energy. For the case of our modeled topological insulator (TI) system, the hexagonal warping and non-linearity increases the rate at which s and s' change as a function of momentum, therefore increasing the overlap of $\langle s| \hat{j}_x |s'\rangle$, and the corresponding conductivity at higher wavenumbers.

Within the framework of Kubo formalism, and taking into account the spin and momentum locking in TIs [2], we calculated the optical conductivity, assuming a surface state dispersion of:

$$E(k, \theta) = \beta k^2 \pm \sqrt{v_0^2 k^2 + \lambda^2 k^6 \cos^3(3\theta)}. \tag{S3}$$

The parameters β and v_0 are the quadratic and linear component of the dispersion, respectively, while λ is related to the hexagonal warping. Eqn. S3 is similar to that used in [3], with the addition of a quadratic correction. Utilizing the relationship between momentum and spin of SS carriers [2], the wavefunction of the SS charge carriers can be determined and evaluated in the Kubo framework, described by Eqn. S1. Moreover, when E_F is at the Dirac point ($E_F = 0$), interband transitions are allowed at all energies. The resulting conductivity is then given by:

$$\sigma_1(\omega) = \frac{e^2}{32\hbar\pi\omega^2} \int_0^{2\pi} v_0^2 k^2 \frac{\omega^2/4 - 2\lambda^2 k^6 \cos^3(3\theta) + 9\lambda^2 k^6}{\omega^2/4 + 2\lambda^2 k^6 \cos^3(3\theta)} d\theta, \tag{S4}$$

where k is a function of θ, and is obtained by solving the equation

$$v_0^2 k^2 + \lambda^2 k^6 \cos^3(3\theta) = \frac{\omega^2}{4}. \tag{S5}$$

A closed form of $\sigma_1(\omega)$ can then be obtained by expanding about small λ. This derivation was guided in large part by prior theoretical work on the optical response of Dirac electron systems [3–5].

II. EXTENDED SUM RULE ANALYSIS OF SURFACE STATES

The modifications to the optical conductance described in the previous section are useful for extending the sum rule constraint, described in the main text, to systems characterized by hexagonal warping and band asymmetry. Accordingly, we have considered the optical conductance arising from three different SS dispersions, shown in Fig. S1a, S1b and S1c. The dispersion shown in Fig. S1a is the same as that used in the main text for establishing the sum rules. In Fig. S1b, the dispersion is modified to include minor hexagonal warping, and a smaller v_0. Lastly, in Fig. S1c, we show the surface state dispersion of an n-type $(Bi_{0.5}Sb_{0.5})_2Te_3$ crystal, extracted from photoemission data in [6], which was characterized by significant hexagonal warping and band asymmetry. Although not comprehensive, examining these dispersions and their corresponding optical response may provide some intuition as to how features of the SS dispersion influence the optical conductance.

In these schematics, we have also indicated the bulk band dispersion with the blue dotted lines. The bulk band structure we show is based on combined photoemission and transport [6–8]. These data indicate the presence of a light and heavy hole band that are both offset from the Γ-point, and an electron band centered in the Brillouin zone. The relative positioning of E_F, the Dirac point, and the bulk bands in Fig. S1a and S1b illustrate scenarios consistent with our experimental observation of p-type carriers. The alternative n-type picture that was measured in [6] is illustrated in Fig. S1c.

The conductance spectra, calculated when $E_F = 0$, corresponding to the SS dispersions shown in Fig. S1a,S1b and S1c are plotted as the dotted line in Fig. S1d, S1e and S1f, respectively. However, the schematic shown in Fig. S1a-c shows E_F shifted away from the Dirac point, yielding a system where hole (electron) states are depopulated

(populated), as in Fig. S1a and S1b (Fig. S1c). For interband transitions to occur in these systems, it must be possible to excite an electron from a populated hole state, to a depopulated electron state, while conserving momentum ($\vec{k}$). Thus, the populated or depopulated states block interband transitions below a threshold energy (ω_{th}). For symmetric bands, $\omega_{th} = 2|E_F|$. In an asymmetric SS dispersion, ω_{th} must be determined on a case by case basis. The blocked interband transitions below ω_{th} suppresses the optical conductance. However, the f-sum rule, described in the main text demands that spectral weight cannot be lost, but is instead transferred into the Drude oscillator. The conductance spectra corresponding to the schematics in Fig. S1a-c, where $|E_|F = E_g$, are indicated by the solid lines in Fig. S1d-f, respectively.

A salient feature in these conductance spectra is that increasing the hexagonal warping, increases the upturn in Conductance as ω increases. Accordingly, a higher hexagonal warping corresponds to a larger area of suppressed spectral weight, resulting in a larger Drude spectral weight (D), which is indicated in Fig. S1d-f. In addition, for comparison with our experimental data, we can extract the SS carrier density (n_{SS}) from the extracted SS dispersion via:

$$n_{SS} = \frac{1}{8\pi^2}\int_0^{2\pi} k_F^2(\theta)d\theta.$$

Since we are probing two surfaces, the total two dimensional carrier density (n_{2D}) is given by $n_{2D} = 2 \cdot n_{SS}$, and is indicated in Fig. S1d-f. The experimentally obtained values were $D^{exp} = 0.13meV$ and $n_{2D}^{exp} = 1.3 \times 10^{13} cm^{-2}$. The schematic shown in Fig. S1a predicts D and n_{2D} values that closely match what was measured, however, for an exact match E_F would have to be within the bulk valence band. In contrast, slight modifications to the SS dispersion as in Fig. S1b overestimates the values of D and n_{2D} when $|E_F| = E_G$. Instead, our experimental values are reproduced when $|E_F| = 0.19eV$, a value smaller than E_G, suggesting our measurements are consistent with a completely surface dominated response, without bulk contributions. Interestingly, the n-type schematic shown in Fig. S1c corresponds to a D even larger than what we measured, but significantly underestimates n_{2D}, due to the reduced area of the Fermi surface. Thus, this picture is inconsistent with our measurements.

III. COMPARISON OF D AND n_{2D} FOR LINEAR SS BANDS

In the main text, our analysis of D and n_{2D}, implied an $|E_F|$ of 221 meV, thereby suggesting E_F resides 16 meV in the bulk valence band (BVB). However, this estimate is incomplete since it neglects contributions to D and n_{2D} from the bulk bands, which are significant when E_F is at the edge of the (BVB). To illustrate this latter effect, we have seperately calculated D and n_{2D}, as a function of E_F for the three elements comprising the composite system: SS bands, the light hole band (LHB), and the heavy hole band (HHB). The effective masses of the LHB and the HHB, as well as their relative position, were taken from [7, 8] and used to assemble the schematic band structure shown in Fig. S2a. To calculate D and n_{2D} from this schematic band structure, we utilized the well known relationships between m^*, E_F, n_{2D} and D for bulk bands [9–11], and the analagous relationships for linear bands detailed in the main text. The resulting E_F dependent values of D and n_{2D} are plotted in Fig. S2b and S2c, respectively. The black, red, and green lines indicate the individual contribution from the SS, the LHB and the HHB, respectively. The value of D or n_{2D} that we would expect to measure is the sum of these these latter three contributions, which is indicated by the dotted gray line. Lastly, the blue line indicates our experimentally obtained value. Therefore, a more realistic value of E_F, where the combined bulk and surface contributions are taken into account corresponds to the point where the dotted gray line intersects the blue line. In the case of the D, the intersection occurs at E_F=211 meV, which is only 5 meV into the LHB. The total carrier density corresponding to this value E_F is $1.16\times10^{13}\text{cm}^{-2}$, in close agreement with our experimentally measured value of $1.28 \times 10^{13}\text{cm}^{-2}$. Moreover, the surface carriers in this scenario account for approximately 98% of the total carriers, suggesting a highly surface dominated response.

Alternatively, we considered the possibility that the carriers we measure arise solely from the bulk bands, where the resulting E_F dependent D and n_{2D} spectra are plotted in Fig. S2d and S2e, respectively. Again, the red and green lines indicate the contributions from the LHB and the HHB, and the sum of these two bulk contributions is the dotted gray line. In these plots, the dotted gray line intersects the measured D at $E_F = 30\text{meV}$. However, this value of E_F would imply an n_{2D} of $5 \times 10^{12}\text{cm}^{-2}$, less than half of what was measured. In fact, it was found that neither of the bulk valence bands, in isolation, could consistently reproduce our measured D and n_{2D} values. Even so, it was possible to adjust the relative positioning of these bands could produce a multi-band response that matches our measurements. However, such a multi-band system would contradict the linear behavior of the Hall resistance, discussed in the main text, which indicates a single carrier species. This analysis emphasizes the notion that our data can be consistently described by assuming a SS dominated response, but not bulk.

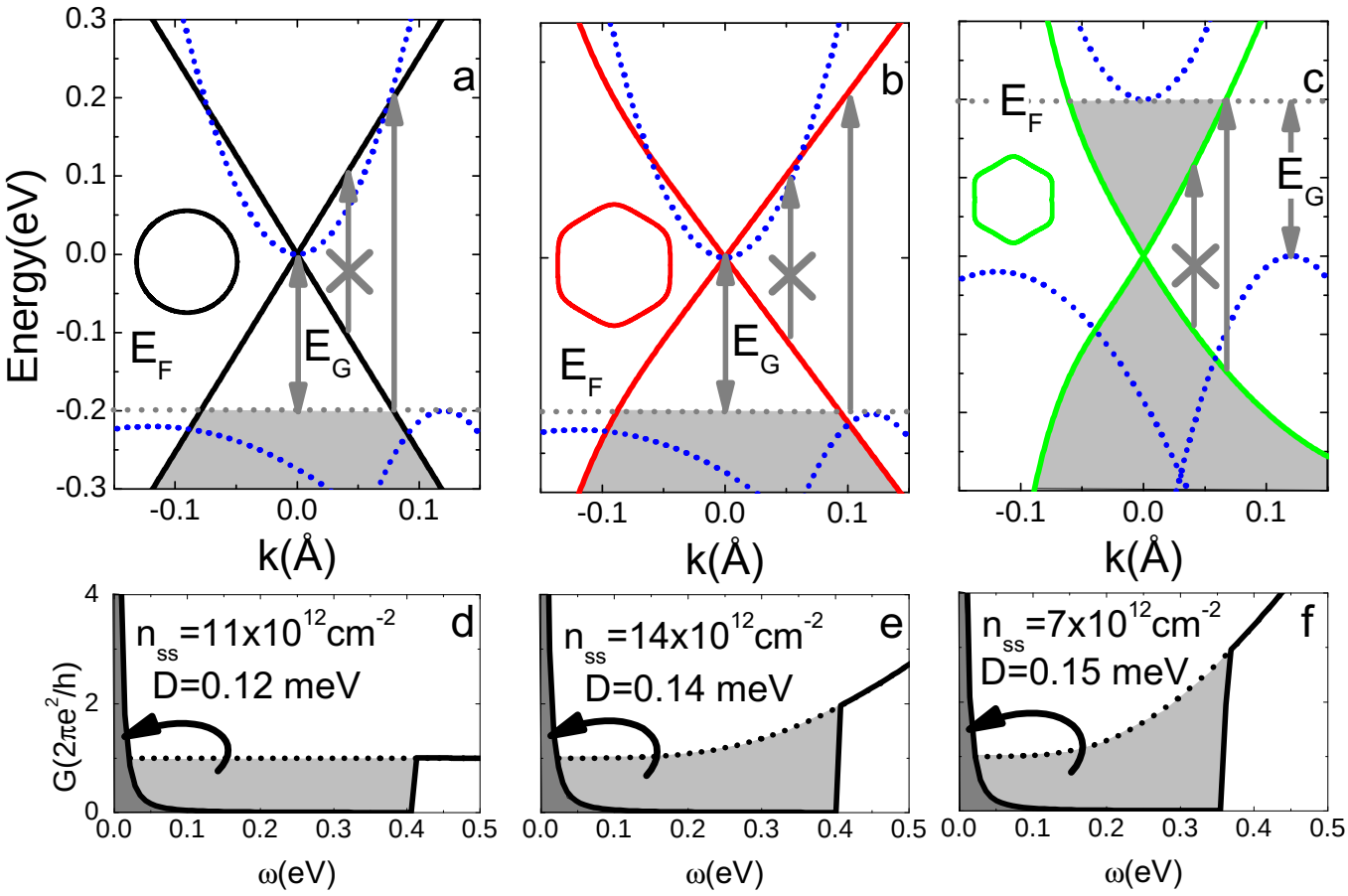

FIG. S1. Panels (a), (b) and (c) schematically show the SS dispersion and bulk band structure corresponding to different experimental scenarios. (a) shows a SS dispersion without hexagonal warping, where the Dirac point is at the bottom of the bulk conduction band. (b) shows a dispersion similar to (a), with the addition of minor hexagonal warping and a slightly smaller v_0. (c) shows the SS dispersion, extracted from [6], where the Dirac point as at the same energy as the bulk valence band, and E_F is at the bottom of the bulk conduction band. The optical conductance corresponding to each of the schematics (a), (b) and (c), are shown in (d), (e) and (f), respectively. In (d),(e) and (f), the dotted line shows the predicted conductance when E_F is at the Dirac point, whereas the solid line indicates the conductance expected when $|E_F| = E_G$, as indicated in the corresponding schematics.

IV. DRUDE-LORENTZ FITTING OF THE CONDUCTANCE SPECTRA

In the main text, only the Drude-Lorentz fitting of the 8K conductance data was shown. The same fitting procedure was employed to extracte the value of D and scattering time τ for all data sets that are shown in Fig. 2c and 2d of the main text. For completeness, the Drude-Lorentz fits to the conductance spectra at all measured temperatures are shown in Fig. S3

The most prominent features of these spectra are the two phonons at 6 meV and 8 meV. The lower energy resonance has a center frequency in close agreement with the E_u^1 phonon mode of Bi_2Te_3 [12], while the weaker higher energy mode has two possibilities. The center frequency of this latter mode suggests assignment to either the E_u^1 mode of Sb_2Te_3, or the A_{1g}^1 mode, which is at similar energies in both stoichiometric compounds [12]. The A_{1g}^1 mode is typically only Raman active, however, this mode may become IR active in the $(Bi,Sb)_2Te_3$ alloy due to the broken translational symmetry introduced via Bi:Sb substitution.

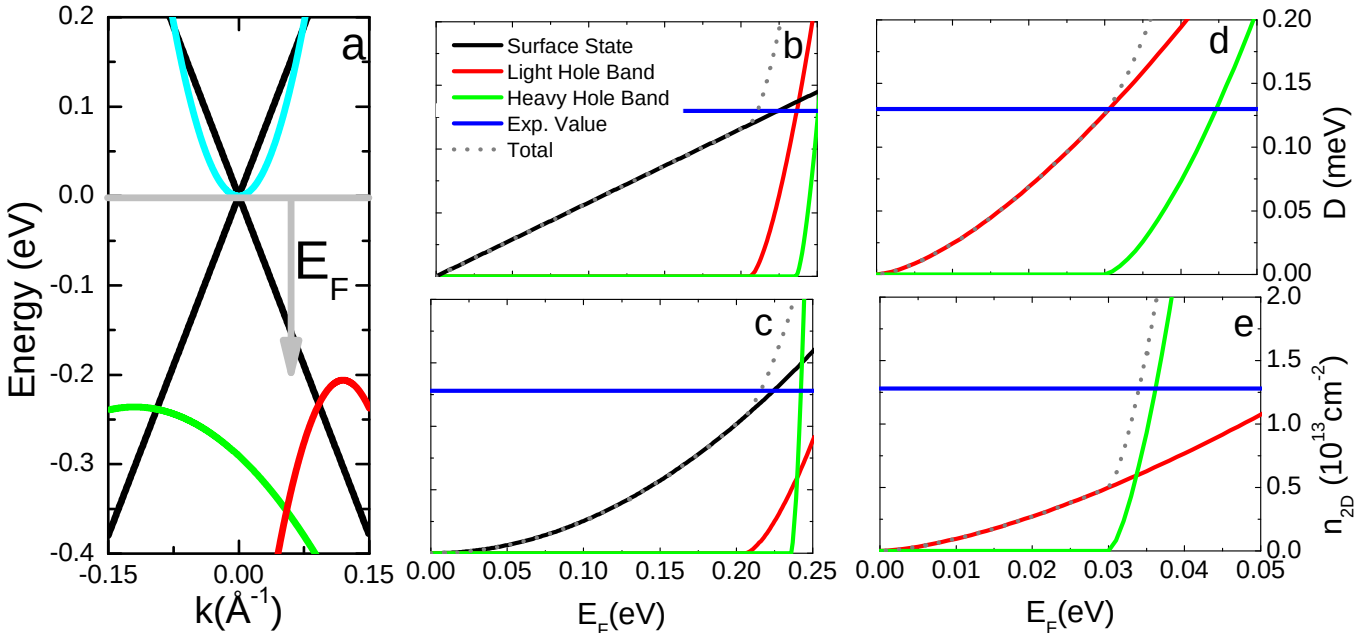

FIG. S2. A schematic band structure of the measured $(Bi,Sb)_2Te_3$ thin film is shown in (a). The surface state band, the conduction band, the light hole band and the heavy hole band are indicated by the black, cyan, red and green lines, respectively. The E_F dependent values of D and n_{2D} that would be expected to arise from the composite bulk and surface response of this system are plotted in (b) and (c), respectively. In (b) and (c), E_F is defined relative to the Dirac point. Alternatively, the E_F dependent D and n_{2D} that would be expected in the absence of the SSs are plotted in (d) and (e), respectively. In these latter two panels, E_F is defined relative to the top of the light hole band. In panels (b-e) the blue line indicates the experimentally measured value, while the black, red and green lines indicate the isolated contribution to the D or n_{2D} spectra from the SS, the light hole band and the heavy hole band respectively while the dotted gray line indicates the sum of these latter three contributions, and the value that we would expect to measure.

V. SAMPLE GROWTH

The $(Bi,Sb)_2Te_3$ films in this study were prepared using molecular beam epitaxy, with a composition of approximately 54% Sb to 46% Bi. These films were grown along the c-axis with a thicknes of 58nm on an insulating InP (111) substrate, where the InP oxide was desorbed under a flux of As to retain a smooth surface for the TI growth. Our films were grown under a Te overpressure, with a Te/(Bi+Sb) beam equivalent pressure ratio of about 7. These growth conditions were determined to yield samples that could be gated through the Dirac point, and possessed insulating resistance vs. temperature curves. The film was capped with a 10nm insulating amorphous Se layer at room temperature, which prevents oxidation and has negligible effects on low energy optical spectroscopy measurements, as demonstrated in [13]. We confirmed the opticaly inert nature of the Se capping layer by also measuring an InP substrate with a thin layer of Se, and comparing it to bare InP. Further characterization of the film was done using x-ray diffraction, and low temperature magneto-transport. Likewise, the film thickness was determined by X-ray reflectivity, and the composition by secondary ion mass spectroscopy measurements on similar samples.

VI. SPECTROSCOPIC TECHNIQUE

The energy range covered by the Terahertz-Time domain spectroscopy (THz-TDS) and fourier transform infrared (FTIR) experiments are roughly 2-10 and 5-900 meV, respectively. The complex, frequency dependent optical constants of the film ($\tilde{\epsilon}(\omega)$,$\tilde{n}(\omega)$,$\tilde{\sigma}(\omega)$, which are all algebraically related [1]), were determined seperately for the THz-TDS and FTIR experiments, and then merged together. To obtain the optical constant of the film for this two layer system (film+substrate), it was necessary to first precisely determine the optical constants of the InP substrate at each temperature. For the FTIR data, we constructed a multi-layer, multi-oscillator, Kramers-Krònig consistet model fit of the raw transimssion data, yielding the optical constants of the film [14]. In the THz-TDS experiment, we measure

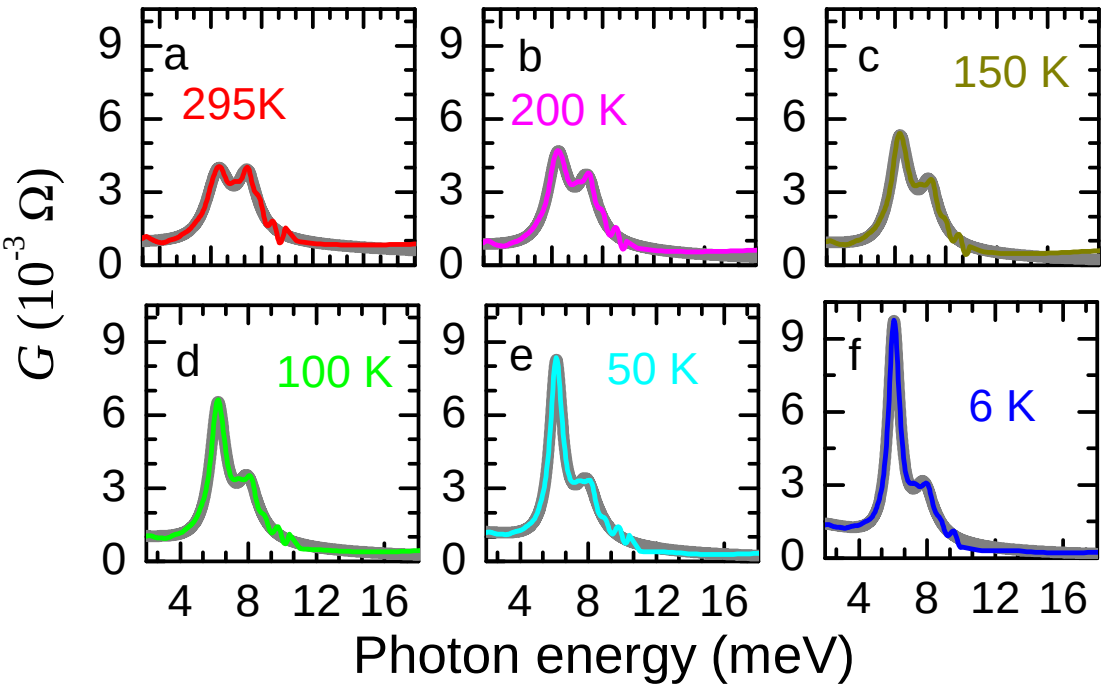

FIG. S3. The experimental conductance spectra of $(Bi,Sb)_2Te_3$ (colored lines) are shown for all measured temperatures, along with the Drude-Lorentz fit (gray lines).

the time-resolved transmitted electric field, from which the optical constants are calculated directly [15].

VII. ENERGY GAP

Establishing the maximum Drude spectral weight required a value for E_G, which can be readily determined from our data. In Fig. S4a we plot $(\epsilon_2(\omega))^2$ from 75-900 meV, where $\epsilon_2(\omega)$ is the imaginary part of the complex, frequency dependent dielectric function, $\tilde{\epsilon}(\omega) = \epsilon_1(\omega) + i\epsilon_2(\omega)$. E_G is found from the x-intercept of a linear fit to $(\epsilon_2(\omega))^2$ in the linear onset regime, $\simeq 200 - 250$ meV [16]. The resulting value of E_G is plotted as a function of temperature in Fig. S4b. The data show a relatively temperature independent E_G of 206.5±3.4 meV, in contrast to the significant temperature dependence of E_G observed in other works [17]. Also noticeable in the $(\epsilon_2(\omega))^2$ spectra are distinct resonant features at $\omega > E_G$, which are suggestive of Van Hove singularities in the $(Bi,Sb)_2Te_3$ band structure, but are not discussed in detail in this work [16].

VIII. THREE LAYER MODEL OF THE TI SYSTEM

Our method of extracting the optical constants, and thus D, are consisten with silimar analysis in the literature [13, 18, 19]. However, an assertion of SS conductance requires a 3-layer model for the TI film, *i.e.* two conductive surfaces and one insulating bulk layer, whereas in the main text, the value of D is extracted using a model consisting of one layer and a single Drude, where a single layer accounts for the effect of both surfaces. Thus, to confirm the plausibility that theDrude conductance is due to SS electrons, the THz-TDS transmission was alternatively modeled assuming 3-layers + substrate: (1) 1 nm surface layer, (2) 58 nm bulk layer, (3) 1 nm surface layer, and (4) 0.5 mm InP substrate, as illustrated schematically in Fig. S5. The Se capping layer was neglected since, as stated earlier, it was found to have a negligible effect on the optical response of the system. We ascribe single (identical) Drude oscillators to layers (1) and (3), with the bulk layer (2) having two lorentzian oscillators to describe the phonons. The choice of 1nm for the surface layers is based on theoretical predictions [20], though the choice in SS thickness

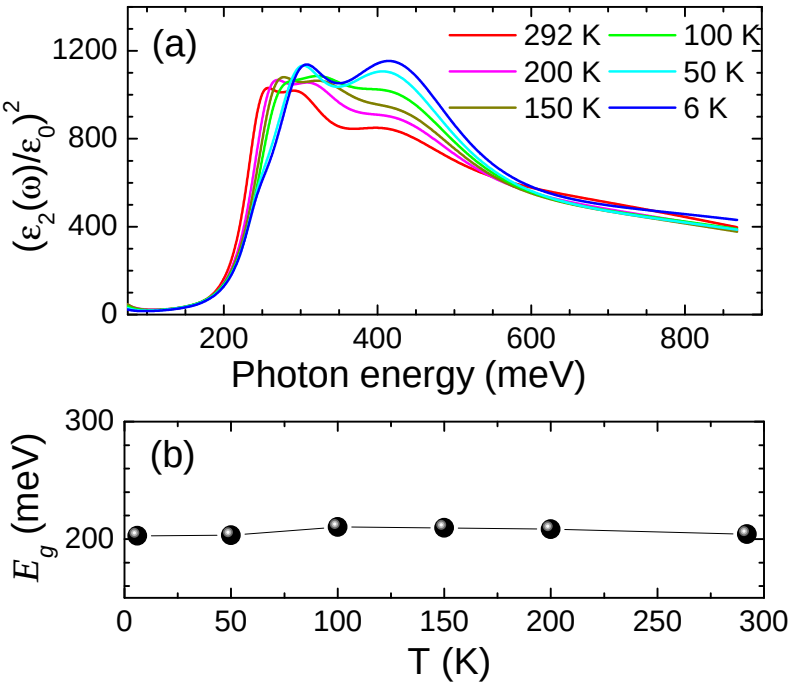

FIG. S4. Panel (a) shows the $(\epsilon_2/\epsilon_0)^2$ spectra at all measured temperatures, where the lienar region near 200 meV indicates the onset of interband transitions. The magnitude of E_G is extracted from these spectra using a linear fit to $(\epsilon_2/\epsilon_0)^2$ where teh x-axis intercept corresponds to the value of E_G. E_G extracted using this procedure is plotted as a function of temperature in (b).

has negligible effect, as long as it is much less than the optical penetration depth [21]. Under this 3-layer modeling, the D extracted for each surface of the 6K THz-TDS transmission is 0.07 meV, for a total (D^s_{3layer}) of 0.14 meV. This is in good agreement with D=0.13 meV extracted from the conductance that was calculated directly from the THz-TDS data. The agreement between these two methods, and the proximity to the threshold of D^s_{max}, confirms the plausibility that the Drude conductance observed is dombinated by the topological SSs.

IX. BOLTZMANN DERIVATION OF THE DRUDE SPECTRAL WEIGHT

The f-sum rule analysis, detailed in the main text, offers an intuitive way to understand limits on the Drude spectral weight in Dirac systems. However, the value of D can be alternatively derived using the Boltzmann equation, which requires only that the shape of the Fermi surface is known, rather than the entire band structure. With this knowledge of the Fermi surface, σ_{xx} is given by the Boltzmann equation:

$$\sigma_{xx} = \frac{e^2}{i\omega - 1/\tau} \int v_x^2 \frac{k_F}{|\partial E/\partial k|} d\phi \tag{S6}$$

where D is given by:

$$D = e^2 \int v_x^2 \frac{k_F}{|\partial E/\partial k|} d\phi. \tag{S7}$$

With this equation, D can be calculated simply from the SS dispersion, given by Eqn. S3. We therefore extracted the SS dispersion of a number of TI systems from photoemission data, which are shown in Fig. S6b, with the corresponding Fermi surface at $E_F = E_G$ shown in Fig. S6c. The resulting values of D are plotted as a function of E_F in Fig. S6c, with the energy gap of the different materials indicated by the arrows, colored to match their respective system. Using the same reasoning as in the main text, the estimated maximum value of D without bulk contributions is achieved when $E_F = E_G$. The maximum values of D obtained from the Boltzmann derivation ($D^s_{Boltz,max}$) are shown next to the experimentally obtained values of D in Table I, a modified verion of the table shown in the text. The results of this complementary analysis of D are consistent with our previous conclusions.

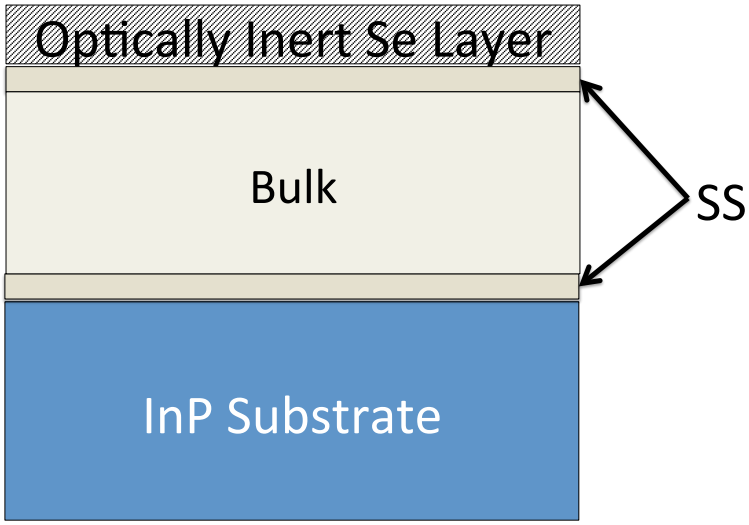

FIG. S5. A schematic of the 3 layer BST+Substrate model that was used for extracting D. The top Se capping layer is optically inert, and was thus not considered in the model. The BST SS layers consisted ofa single Drude oscillator, with identical values of D and τ. The model for the BST bulk included only two lorentzian oscillators to capture the phonon modes. The InP substrate was measured and characterized separately, without the BST system.

TABLE I. Bulk band gap E_g, experimental Drude oscillator strength D^{exp} from transmission based experiments, modeled Drude oscillator strength D^s_{3layer} where conductance is assumed to be from 2 topological surfaces with an insulating bulk, and theoretical upper bound of the Drude oscillator strength $D^s_{\text{Boltz,max}}$ of prototypical strong TIs obtained using the bulk energy gap, and the SS dispersion shown in Fig. S6a. Values of D are all taken from low-temperature data (6–20 K). All units are meV. †The results of Ref.[21] are from reflection based experiments, and thus only one topological surface is considered.

TI material	E_g	D^{exp}	D^s_{3layer}	$D^s_{\text{Boltz,max}}$	Refs.
Bi_2Se_3	300	0.09–0.70	–	0.17	[13, 18, 24, 27]
Bi_2Te_3	142	1.26	–	0.09	[10]
$Bi_{1.5}Sb_{0.5}Te_{1.8}Se_{1.2}$	340	1.42	–	0.34	[19]
Bi_2Te_2Se†	290	–	0.83	0.14	[21]
$Bi_{0.92}Sb_{1.08}Te_3$	207	0.13	0.14	0.15	This work

[1] M. Dressel and G. Gruener, *Electrodynamics of Solids: Optical Properties of Electrons in Matter*, vol. 70 (Cambridge University Press, New York, New York, USA, 2002), 1st ed., ISBN 0 511 01439 2.

[2] C.-X. Liu, X.-L. Qi, H. J. Zhang, X. Dai, Z. Fang, and S.-C. Zhang, Phys. Rev. B **82**, 045122 (2010), URL `http://link.aps.org/doi/10.1103/PhysRevB.82.045122`.

[3] Z. Li and J. P. Carbotte, Physical Review B **87**, 155416 (2013), ISSN 1098-0121, URL `http://link.aps.org/doi/10.1103/PhysRevB.87.155416`.

[4] B. Wunsch, T. Stauber, F. Sols, and F. Guinea, New Journal of Physics **8**, 318 (2006), ISSN 1367-2630, URL `http://stacks.iop.org/1367-2630/8/i=12/a=318?key=crossref.1ac84bfc3f85e7367b9a281336c35735`.

[5] L. Fu, Physical Review Letters **103**, 266801 (2009), ISSN 0031-9007, URL `http://link.aps.org/doi/10.1103/PhysRevLett.103.266801`.

[6] D. Kong, Y. Chen, J. J. Cha, Q. Zhang, J. G. Analytis, K. Lai, Z. Liu, S. S. Hong, K. J. Koski, S.-K. Mo, et al., Nature nanotechnology **6**, 705 (2011), ISSN 1748-3395, URL `http://www.ncbi.nlm.nih.gov/pubmed/21963714`.

[7] V. Kulbachinskii, V. Kytin, P. Tarasov, and N. Yuzeeva, Physics of the Solid State **52**, 1830 (2010).

[8] V. Kulbachinskii, Z. Dashevskii, M. Inoue, M. Sasaki, H. Negishi, W. Gao, P. Lostak, J. Horak, and A. de Visser, Phys. Rev. B **52**, 10915 (1995).

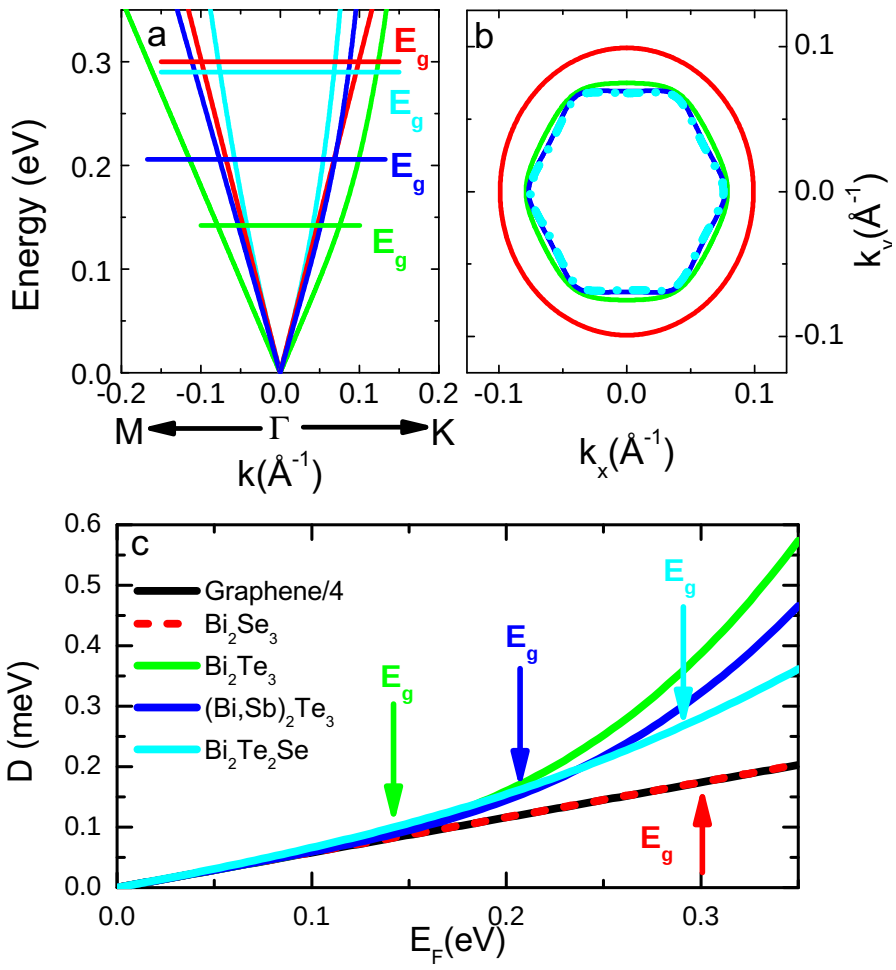

FIG. S6. The SS dispersion above the Dirac point, which was extracted from photoemission data [6, 22–26], is shown in (a) for four different TI systems. The lines, colored to match their respective system, indicate the bulk energy gap, with the Fermi surface corresponding to $E_F = E_G$ plotted in (b). The value of D, extracted from the SS dispersion using Eqn. S7, is plotted as a function of E_F in (c), with the bulk energy gap indicated by the arrows, colored to match their respective system.

[9] D. N. Basov, R. D. Averitt, D. van der Marel, M. Dressel, K. Haule, and C. Gene, Reviews of Modern Physics **83**, 471 (2011), ISSN 0034-6861, URL http://link.aps.org/doi/10.1103/RevModPhys.83.471.

[10] B. C. Chapler, K. W. Post, a. R. Richardella, J. S. Lee, J. Tao, N. Samarth, and D. N. Basov, Physical Review B **89**, 1Fr (2014), ISSN 1550235X, 1405.4916.

[11] C. Kittel, *Introduction to Solid State Physics* (2005), 8th ed.

[12] W. Richter, H. Kohler, and C. Becker, Phys. Stat. Sol. (b) **84**, 619 (1977).

[13] L. Wu, M. Brahlek, R. Valdés Aguilar, a. V. Stier, C. M. Morris, Y. Lubashevsky, L. S. Bilbro, N. Bansal, S. Oh, and N. P. Armitage, Nature Physics pp. 1–5 (2013), ISSN 1745-2473, URL http://www.nature.com/doifinder/10.1038/nphys2647.

[14] A. B. Kuzmenko, Review of Scientific Instruments **76**, 083108 (2005), ISSN 00346748, URL http://link.aip.org/link/RSINAK/v76/i8/p083108/s1&Agg=doi.

[15] R. D. Averitt and A. J. Taylor, Journal of Physics: Condensed Matter **14**, R1357 (2002).

[16] R. Yu, W. Zhang, H.-J. Zhang, S.-C. Zhang, X. Dai, and Z. Fang, Science (New York, N.Y.) **329**, 61 (2010), ISSN 1095-9203, URL http://www.ncbi.nlm.nih.gov/pubmed/20522741.

[17] K. W. Post, Y. S. Lee, B. C. Chapler, A. A. Schafgans, M. Novak, A. A. Taskin, K. Segawa, M. D. Goldflam, H. T. Stinson, Y. Ando, et al., Phys. Rev. B **91**, 165202 (2015), URL http://link.aps.org/doi/10.1103/PhysRevB.91.165202.

[18] R. Valdés Aguilar, a. V. Stier, W. Liu, L. S. Bilbro, D. K. George, N. Bansal, L. Wu, J. Cerne, a. G. Markelz, S. Oh, et al., Physical Review Letters **108**, 087403 (2012), ISSN 0031-9007, URL http://link.aps.org/doi/10.1103/PhysRevLett.108.087403.

[19] C. S. Tang, B. Xia, X. Zou, S. Chen, H.-W. Ou, L. Wang, a. Rusydi, J.-X. Zhu, and E. E. M. Chia, Scientific reports **3**, 3513 (2013), ISSN 2045-2322, URL http://www.pubmedcentral.nih.gov/articlerender.fcgi?artid=3865466&tool=pmcentrez&rendertype=abstract.

[20] H. Zhang, C.-X. Liu, X.-L. Qi, X. Dai, Z. Fang, and S.-C. Zhang, Nature Physics **5**, 438 (2009), ISSN 1745-2473, URL http://www.nature.com/doifinder/10.1038/nphys1270.

[21] A. A. Reijnders, Y. Tian, L. J. Sandilands, G. Pohl, I. D. Kivlichan, S. Y. F. Zhao, S. Jia, M. E. Charles, R. J. Cava, N. Alidoust, et al., Physical Review B **89**, 075138 (2014), ISSN 1098-0121, URL http://link.aps.org/doi/10.1103/PhysRevB.89.075138.

[22] D. Hsieh, Y. Xia, D. Qian, L. Wray, J. H. Dil, F. Meier, J. Osterwalder, L. Patthey, J. G. Checkelsky, N. P. Ong, et al., Nature **460**, 1101 (2009), ISSN 1476-4687, URL http://www.ncbi.nlm.nih.gov/pubmed/19620959.

[23] M. Neupane, S.-Y. Xu, L. A. Wray, A. Petersen, R. Shankar, N. Alidoust, C. Liu, A. Fedorov, H. Ji, J. M. Allred, et al., Physical Review B **85**, 235406 (2012), ISSN 1098-0121, URL http://link.aps.org/doi/10.1103/PhysRevB.85.235406.

[24] Y. Xia, D. Qian, D. Hsieh, L. Wray, A. Pal, H. Lin, A. Bansil, D. Grauer, Y. S. Hor, R. J. Cava, et al., Nature Physics **5**, 398 (2009), ISSN 1745-2473, URL http://www.nature.com/doifinder/10.1038/nphys1274.

[25] Y. L. Chen, J. G. Analytis, J.-H. Chu, Z. K. Liu, S.-K. Mo, X. L. Qi, H. J. Zhang, D. H. Lu, X. Dai, Z. Fang, et al., Science (New York, N.Y.) **325**, 178 (2009), ISSN 1095-9203, URL http://www.ncbi.nlm.nih.gov/pubmed/19520912.

[26] T. Arakane, T. Sato, S. Souma, K. Kosaka, K. Nakayama, M. Komatsu, T. Takahashi, Z. Ren, K. Segawa, and Y. Ando, Nature communications **3**, 636 (2012), ISSN 2041-1723, URL http://www.ncbi.nlm.nih.gov/pubmed/22273674.

[27] L. Wu, W.-K. Tse, M. Brahlek, C. Morris, R. Valdés Aguilar, N. Koirala, S. Oh, and N. Armitage (2015), 1502.04577v1.